

ANALYSIS AND CLASSIFICATION OF KIDNEY FOCAL LESIONS FROM B-MODE ULTRASOUND IMAGES

*Dissertation submitted in partial fulfillment of the requirements for the Degree
of*

MASTERS OF TECHNOLOGY IN ELECTRONICS & COMMUNICATION ENGINEERING

By

SHAILJA RANA
Enrollment No. 142007

UNDER THE GUIDANCE OF

Dr. SHRUTI JAIN



JAYPEE UNIVERSITY OF INFORMATION TECHNOLOGY, WAKNAGHAT, SOLAN,
HIMACHAL PRADESH- 173234

May 2016

TABLE OF CONTENTS

CONTENTS	PAGE NO.
DECLARATION BY THE SCHOLAR	iv
SUPERVISOR'S CERTIFICATE	v
ACKNOWLEDGEMENT	vi
ABSTRACT	vii
LIST OF FIGURES	ix
LIST OF TABLES	x
LIST OF ACRONYMS	xi
CHAPTER 1	
INTRODUCTION	
1.1 Overview	1
1.2 Ultrasound (US)	6
1.3 Need of Computer Aided Diagnosis (CAD) Systems	7
1.4 Objective of the Project Work	8
CHAPTER 2	
LITERATURE REVIEW	
2.1 Overview	9
2.2 Different CAD System Designs for the Classification of Kidney US Images	9
2.3 Concluding Remarks	12
CHAPTER 3	
METHODOLOGY	
3.1 Introduction	13
3.2 General CAD System Design	13
3.2.1 Dataset Collection and Description	15
3.2.2 Area of Interest (AOI) Selection Protocol	15
3.2.3 Feature Extraction Module	16
3.2.3.1 Statistical Texture Features	17
3.2.3.1.1 First Order Statistics Features	17
3.2.3.1.2 Second Order Statistics Features (GLCM)	17
3.2.3.1.3 Higher Order Statistics Features (GLRLM)	18
3.2.3.1.4 Other Statistical Features	18
3.2.3.2 Spatial Filtering Based Texture Features	19
3.2.3.3 Spectral Texture Features	20
3.2.3.3.1 2-D Gabor Wavelet Transform Features	20

3.2.3.3.2	Fourier Power Spectrum (FPS) Features	21
3.2.3.3.3	2-D Discrete Wavelet Transform Features	21
3.2.4	Classification Module	22
3.2.4.1	k-Nearest Neighbor (kNN) Classifier	22
3.2.4.2	Probabilistic Neural Network (PNN) Classifier	23
3.2.4.3	Support Vector Machine (SVM) Classifier	23
3.2.4.4	Classifier Performance Evaluation Criteria	24
3.3	Concluding Remarks	25

CHAPTER 4

CAD SYSTEM DESIGN FOR CLASSIFICATION OF FOCAL KIDNEY LESIONS USING GABOR WAVELET TEXTURE FEATURES

4.1	Introduction	26
4.2	Proposed CAD System Design	26
4.2.1	Dataset Description Module	28
4.2.2	AOI Extraction Module	28
4.2.3	Feature Extraction Module	29
4.3	Results and Discussion	30
4.3.1	To obtain the classification performance of spectral features for primary benign (AML) and primary malignant (RCC) kidney lesions using SVM classifier.	30
4.4	Concluding Remarks	31

CHAPTER 5

CAD SYSTEM DESIGN FOR CHARACTERIZATION OF FOCAL KIDNEY LESIONS USING STATISTICAL AND SPECTRAL TEXTURE FEATURES

5.1	Introduction	32
5.2	Proposed CAD System Design	32
5.2.1	Dataset Description Module	33
5.2.2	AOI Extraction Module	34
5.2.3	Feature Extraction Module	35
5.3	Results and Discussion	37
5.3.1	Experiment 1: To find the classification performance of statistical features for primary benign (AML) and primary malignant (RCC) kidney lesions using SVM classifier.	37
5.3.2	Experiment 2: To find the classification performance of spectral features (FPS features) for primary benign (AML) and primary malignant (RCC) kidney lesions using SVM classifier.	38
5.3.3	Experiment 3: To find the classification performance of combined texture features ((GLRLM + FPS) features) for primary benign (AML) and primary malignant (RCC) kidney lesions using SVM classifier.	39
5.4	Concluding Remarks	40

CHAPTER 6

CAD SYSTEM DESIGN FOR CLASSIFICATION OF FOCAL KIDNEY LESIONS USING WAVELET BASED TEXTURE DESCRIPTORS

6.1	Introduction	41
6.2	Proposed CAD System Design	41
6.2.1	Dataset Description Module	42
6.2.2	AOI Extraction Module	43
6.2.3	Feature Extraction Module	43
6.2.3.1	Haar Wavelets (db1)	45
6.2.3.2	Daubechies wavelets (db)	45
6.2.3.3	Symlets Wavelets	45
6.2.3.4	Coiflets Wavelets	45
6.2.3.5	Biorthogonal Wavelets	45
6.3	Results and Discussion	46
6.3.1	To obtain the classification performance of seven wavelet energy descriptors (TFV1-TFV7) derived from compact support wavelet filters for two classes (AML and RCC) of kidney using SVM classifier.	46
6.4	Concluding Remarks	47

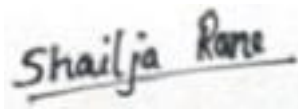
CHAPTER 7

CONCLUSION AND FUTURE SCOPE

7.1	Conclusion	48
7.2	Conclusion: Design of an Efficient CAD System for Classification of Focal Kidney Lesions Using Texture Features	48
7.3	Limitations and Future Scope	49
	Publications from the Present Work	51
	References	52
	Appendix-A: Texture Features Used in the Present Work	60

DECLARATION BY THE SCHOLAR

I hereby declare that the work reported in the M-Tech thesis entitled “**Analysis and Classification of Focal Kidney Lesions from B-Mode Ultrasound Images**” submitted at **Jaypee University of Information Technology, Wagnaghat India**, is an authentic record of my work carried out under the supervision of **Dr. Shruti Jain**. I have not submitted this work elsewhere for any other degree or diploma.



Shailja Rana

Department of Electronics and Communication Engineering

Jaypee University of Information Technology, Wagnaghat, India

Date: 25-05-2016

SUPERVISOR'S CERTIFICATE

This is to certify that the work reported in the M-Tech. thesis entitled “**Analysis and Classification of Focal Kidney Lesions from B-Mode Ultrasound Images**”, submitted by **Shailja Rana** at **Jaypee University of Information Technology, Wagnaghat, India**, is a bonafide record of her original work carried out under my supervision. This work has not been submitted elsewhere for any other degree or diploma.



Signature of Supervisor

Dr. Shruti Jain

Assistant Professor

Date: 25-05-2016

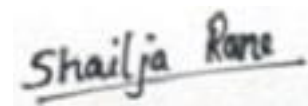
ACKNOWLEDGEMENT

This project work is the most significant accomplishment of my life by far. I would like to extend my gratitude and heartfelt thanks to my supervisor Dr. Shruti Jain, Assistant Professor (Sr. Grade), Department of Electronics and Communication Engineering, Jaypee University of Information Technology, Waknaghat-Solan, for her constant support, encouragement, exemplary guidance and constructive criticism.

I would also like to offer my deepest gratitude to Dr. Jitendra Virmani, Assistant Professor, Department of Electronics and Communication Engineering, Thapar University Patiala, Punjab, for his encouragement, constant support, suggestions and taking out time for answering my questions in carrying out this research that made me to understand the concepts more precisely.

I would also like to thank Dr. Shruti Thakur, Department of Radiology, Indira Gandhi Medical College (IGMC), Shimla, H.P, for meaningful discussions regarding the understanding of sonographic appearances of focal kidney lesions.

Last but not least, I would like to thank my respected parents and my elder brother for their encouragement, patience and support and showing confidence in me throughout my course.



Date 25-05-2016

Signature of Student

ABSTRACT

Recent developments in the computerized analysis of medical images are expected to aid radiologists and other healthcare professionals in various diagnostic tasks of medical image interpretation. Mostly the interpretations of medical images are performed by radiologists. The term computer aided diagnosis (CAD) is defined as, the diagnosis made by the radiologists using the output from a computerized analysis of medical images. This is considered as a “second opinion” in detecting lesions, assessing extent of disease and making diagnostic decisions for improving the interpretation component of medical imaging. Lately, one of the leading research topics in medical imaging and diagnostic radiology is a CAD system. The elementary idea of CAD is to provide a computer output to assist radiologists and other health care experts in reading and understanding the image and to differentiate between various anomalies. With CAD, the final diagnosis is made by the radiologist. Numerous kind of CAD systems are advanced for the detection and classification of various lesions in medical imaging, including X- rays, MRI, CT, and US. It has been noticed that past CAD implementations does not include classification of focal kidney lesions from B-Mode ultrasound images.

The present work focuses on the aspect of textural variations exhibited by primary benign (Angiomyolipomas) and primary malignant (Renal Cell Carcinomas) focal kidney lesions. As an application of texture description in medical area, efficient CAD systems for distinguishing primary focal kidney lesions based on texture features derived from B-Mode kidney ultrasound images has been proposed in the present study. The participating radiologist opined that, on the basis of echogenicity and low fat tissue, it has become difficult to definitely distinguish between small AMLs and small RCCs. When these lesions are smaller (<2cms), they have highly overlapping appearances. So, differentiation between RCCs and AMLs become difficult. Therefore, various CAD systems to appropriately recognize and analyze these abnormalities have been proposed in this research which will help the radiologists in medical environment. This study has been carried out to increase the diagnostic excellence of conventional B-Mode US imaging modality for the diagnosis of kidney diseases. The research objectives for the present work were formulated keeping in view the

needs of the radiologists, based on the practical difficulties faced by them in routine clinical practice.

For the design of this CAD system, image database has been acquired from a publically available source ultrasoundcases.info. From each image, AOIs of fixed and variable sizes has been extracted. The basic CAD system consists of feature extraction module for capturing these textural variations of benign and malignant kidney lesions and the classification module. In the feature extraction module, three methods for extracting the texture features are employed, (a) *Statistical methods* (b) *Spatial Filtering based methods* and (c) *Spectral Texture methods*. In the classification module, the performance of support vector machine (SVM) classifier is evaluated to obtain the class of the unknown testing instances.

By using SVM classifier it is observed that, the CAD system design based on Gabor wavelet texture features achieves maximum classification accuracy of 90.0 % out of all the proposed CAD system designs for the classification of focal kidney lesions. It can be concluded that the Gabor wavelet texture features are thus most useful and efficient texture features to account for the textural variations of focal kidney lesions. Thus, GWT features are considered as best features for differential analysis between primary benign and primary malignant kidney lesions.

LIST OF FIGURES

Figure Number	Title	Page Number
1.1	B-mode ultrasound kidney image.	1
1.2	Echogenic appearance of Ultrasound kidney images. B-mode ultrasound kidney images depicting different cases.	3
1.3	(a) small AML lesion (b) large AML lesion (c) small RCC lesion (d) large RCC lesion B-mode ultrasound kidney images showing different cases.	5
1.4	(a) AML image (b) RCC image	7
3.1	General framework of a CAD system design.	14
3.2	Sample AOI images. (a) Fixed size AOI image (b) Variable size AOI image	16
3.3	Texture features computed for each ROI image. Gabor filters family of 21 wavelets (images) acquired for a sample AML ROI image with scales (0, 1, 2) from top to bottom and	17
3.4	orientations (22.7°, 45°, 67.5°, 90°, 112.5°, 135°, 157.5°) from left to right.	20
3.5	Wavelet depiction of image up to 2nd level of decomposition.	21
4.1	Proposed CAD system design.	27
4.2	Sonographic image of a small AML with marked AOI. Gabor filters family of 21 wavelets acquired for a sample AML	29
4.3	ROI image with 3 scales from top to bottom and 7 orientations from left to right.	30
5.1	Block diagram representation of proposed Computer aided diagnosis system design for two class classification.	33
5.2	Images with marked AOIs. (a) AML image (b) RCC image	34
5.3	Description of dataset for two class classification.	35
5.4	Texture features computed for each AOI image.	36
6.1	Block diagram representation of proposed CAD system design.	42
6.2	Images of extracted AOIs. (a) AML image (b) RCC image	43

LIST OF TABLES

Table Number	Title	Page Number
2.1	Explanation of related studies carried out for kidney image classification.	9
3.1	Description of Laws' masks of different lengths.	19
3.2	Properties of wavelet filters used.	22
4.1	Dataset description for two class classification.	29
4.2	Classification performance of spectral features using SVM classifier for two-class classification.	31
5.1	Description of extracted TFVs for the characterization of AML and RCC lesions.	37
5.2	Description of experiments carried out for two-class breast tissue density classification.	37
5.3	Result of Classification performance of statistical features using SVM classifier for two-classes of Kidney.	38
5.4	Result of Classification performance of Fourier Power Spectrum features using SVM classifier for two-classes of kidney.	39
5.5	Result of Classification performance of combination of statistical and spectral features using SVM classifier for two-classes of kidney.	40
6.1	Description of Seven wavelet energy descriptors as TFVs.	44
6.2	Classification performance of TFVs using SVM classifier.	46
6.3	Classification performance of the best TFVs using SVM classifier.	47
7.1	Performance comparison of CAD system designs for two-class kidney classification using SVM.	48

LIST OF ACRONYMS

AML	Angiomyolipoma
ANN	Artificial Neural Network
AOI	Area of Interest
CAD	Computer Aided Diagnosis
CFV	Combined Feature Vector
CM	Confusion Matrix
DFT	Discrete Fourier Transform
DWT	Discrete Wavelet Transform
FOS	First Order Statistics
FPS	Fourier Power Spectrum
GLDS	Gray Level Difference Statistics
GLCM	Gray Level Co-occurrence Matrix
GLRLM	Gray Level Run Length Matrix
GWT	Gabor Wavelet Transform
ICA	Individual Class Accuracy
kNN	<i>k</i> -Nearest Neighbor
MI	Moment Invariant
MRD	Medical Renal Diseases
NGTDM	Neighborhood Gray Tone Difference Matrix
NN	Neural Network
OCA	Overall Classification Accuracy
PNN	Probabilistic Neural Network
RCC	Renal Cell Carcinoma
SFM	Statistical Feature Matrix
SKT	Segmented Kidney Tissue
SVM	Support Vector Machine
TFV	Texture Feature Vector
US	Ultrasound
WPT	Wavelet Packet Transform

CHAPTER 1

INTRODUCTION

1.1 Overview

The kidneys are a pair of bean-shaped organs, each about the size of a fist, about 10 to 12 cm long, 4 to 6 cm wide, 3 cm thick and weigh 150 g. Their main job is to clean the blood, removing waste products and making urine. They are attached to the upper back wall of the abdomen. One kidney is just to the left and the other just to the right of the backbone probably because of considerable space occupied by the liver. The lower rib cage protects the kidneys. Kidney has parenchyma consisting of outer cortex (outermost portion of the kidney) and inner medulla (innermost part of the kidney). Kidney consists of renal sinus (a fatty section) which is a central area of kidney appear brighter as compared to other part of the kidney images .The basic diagram of kidney ultrasound image is depicted in Figure 1.1.

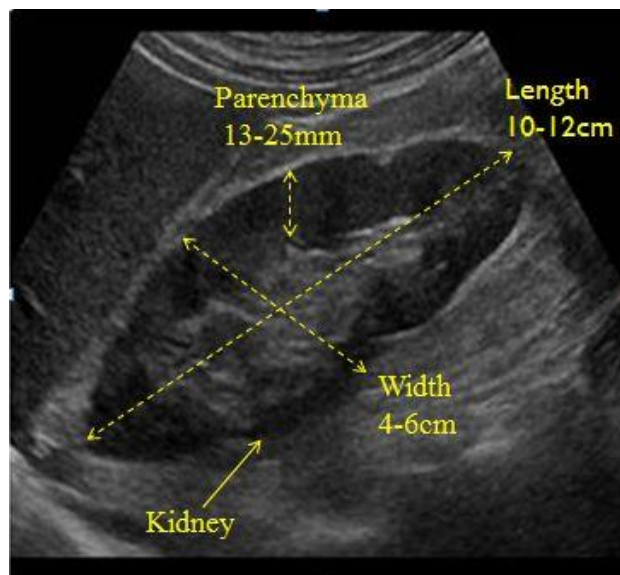


Figure 1.1: B-mode ultrasound kidney image

In human body, the development of tissue masses is the result of uncontrollable growth of cells called tumors. A kidney tumor is an abnormal growth within the kidney. Kidney diseases are considered to be hereditary anomaly or acquired. Kidney tumors are usually solid masses. Kidney tumors are also known as renal tumors. Kidney tumors are considered to be of two types:

(A) Non-Cancerous (Benign tumors)

(B) Cancerous (Malignant tumors)

(A) Non-Cancerous: Benign tumors are non-cancerous. A benign tumor is a mass of cells that lacks the ability to invade neighboring tissue or metastasize which means it does not move (metastasize) to other body parts. Most are asymptomatic, are discovered incidentally, and are not immediately life threatening. Also, benign tumors generally have a slower growth rate.

(B) Cancerous: Malignant tumors are called as cancerous tumors. Malignant tumors are made up of cells having the out of control growth. In these tumors, cells can attack the neighboring tissues and spread to other parts of the body. Sometimes these cancerous cells move away from the original (primary) position of cancer and spread to other body organs where they can continue to produce and form another tumor at that location. This process of spreading of cancerous cells from primary cancerous tumors of the other body parts is termed as metastasis or secondary cancer. Symptoms of malignant tumors are: Blood in urine, weight loss, abdominal pain, high temperatures (fevers) and sweats and a swelling in the area over a kidney.

Nowadays, it is considered as the one of the major problem and is mostly found in people over the age of 60. There are various risk factors which increase the chance that kidney cancer may develop. These include: (a) Age (b) Smoking (c) Obesity (d) Hypertension (e) Genetic factors (f) Chronic kidney failure and/or dialysis (g) Diet with high caloric intake or fried.

In the present study, on the basis of texture patterns and echogenicity, kidney focal lesions are basically divided into following classes: **(1) Primary benign (2) Primary malignant**

Texture pattern is formed by the echo being reflected by the kidney tissues. Here, echogenicity imitates the tissue characteristics of kidney which mean the tissue in relation with another tissue of the kidney or as compared to its normal state. The term echogenicity of kidney means, during ultrasonography the ability of numerous functional parts of kidney to produce echo signals. In other words, echogenicity of tissue is higher when the sound echo is bounced from the surface, reflects increased sound waves. The echogenicity of a kidney nodule states to its brightness compared to the normal kidney parenchyma. Echogenicity can

be hyperechogenic, hypoechogenic and anechogenic. “Hyperechogenic” refers to those tissues having higher echogenicity than normal tissues and they are typically signified with lighter colors on images during medical ultrasonography. In contrast, “Hypoechogenic” refers to those tissues having lower echogenicity than normal tissues and they are generally signified with darker colors. Areas having the absence of echogenicity are termed as “anechogenic” and these are normally shown as completely dark areas during ultrasonography. “Isoechogenic” refers to the tissue having the same echogenicity as the surrounding tissue [1].

The echogenicity of tissue is depicted in Figure 1.2.

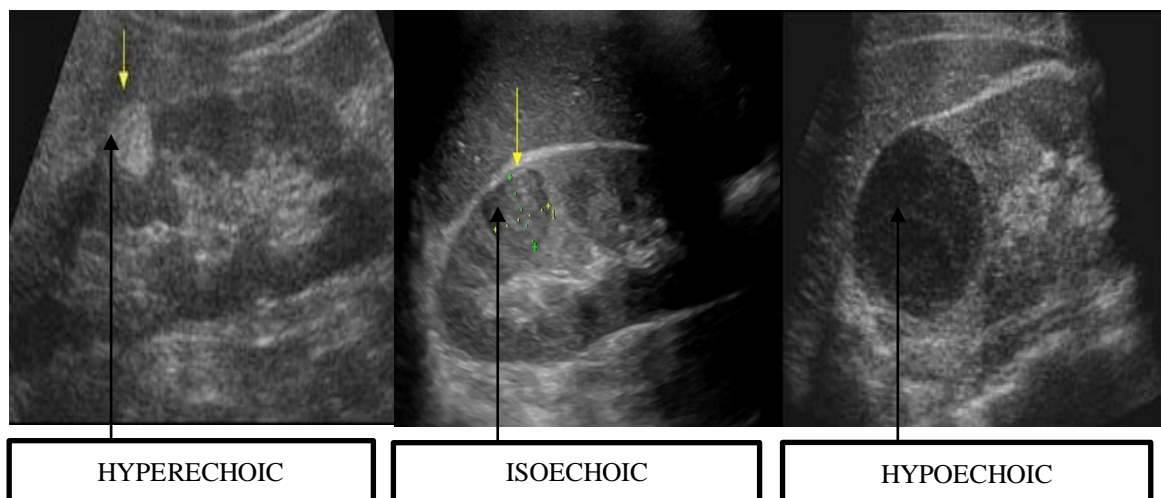


Figure 1.2: Echogenic appearance of Ultrasound kidney images.

The name echogenic is used to define the extent of reverberation (echo) being returned by any structure in relation to surrounding structures. The echogenic appearance of the tumor is mostly related to its fat content and the occurrence of several tissue boundaries within it. Each tumor was evaluated for size, location, echogenicity, homogeneity, shadowing, hypoechoic rim, and intratumoral cysts. The most common occurring kidney focal lesions are described below.

(1) Primary benign: For the present work, benign focal lesion such as AML is considered as primary benign. AML is a most commonly occurring benign tumor in kidney made up of thick blood vessels, fatty and smooth muscle tissue and variable amounts of mature adipose tissue. AML is a most solid frequently encountered solid renal tumor which is common in females. There are mainly two types of renal angiomyolipoma which can be discriminated clinically.

The first type of AML is seen in tuberous sclerosis patients, grows bilaterally, and might have many centres with variable sizes. Angiomyolipoma tumor grows in 80% of tuberous sclerosis cases which is a genetic disease. The second type is a mid-size solitary tumor with unilateral location [2].

In terms of echogenicity, benign tumors are hyperechoic and appear brighter in ultrasound imaging. Therefore, echogenicity is the most distinguishing ultrasonographic feature of AMLs. AMLs are round or egg-shaped cortical tumors and they tend to be well confined, with an echogenicity analogous to that of the echogenic renal sinus. AML is having acoustic shadowing due to intratumoral interferences of high attenuation. AMLs, whose diameter is very small in terms of few millimeters, may be recognized because of their intense echogenicity. A reduction of echogenicity in AML is supposed to be associated with a decrease in the quantity of fat and to an increase in the prominence of myogenic components. AMLs are hyperechoic masses relative to renal parenchyma and may appear less echogenic (hypoechoic) depending on the relative proportion of fat, smooth muscle, vascular components and hemorrhage in lesions. The Ultrasonographic appearance of small size AMLs (<2cms) is hyperechoic and having the homogeneous echotexture and the extent of reverberation being returned by some surface with respect to its normal echo is given by echotexture. For large size AMLs (>2cms) sonographic appearance is hyperechoic, heterogeneous lesions with high echogenicity.

(2) Primary malignant: Among malignant focal lesion, RCC comes under primary malignant. RCC (also known as renal adenocarcinoma) is a kidney cancer that originates in the lining of the proximal convoluted tubule, a part of the very small tubes in the kidney that transport waste molecules from the blood to the urine. RCC is the most common type of kidney cancer in adults, responsible for approximately 90-95% of cases. RCC is also one of the most solid frequently encountered solid renal tumor. RCC has been seen by both intratumoral cysts and hyperechoic rim. The sonographic appearances of kidney tissues based on echogenicity are depicted in Figure 1.3.

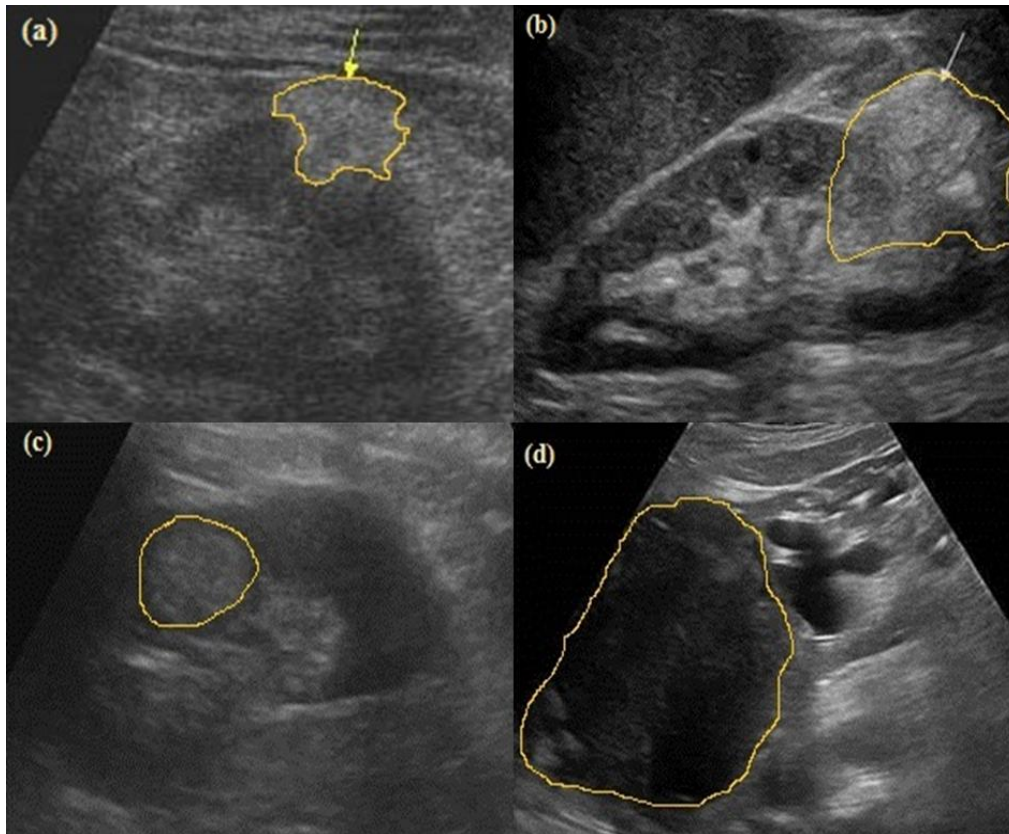


Figure 1.3: B-mode ultrasound kidney images depicting different cases. (a) small AML lesion (b) large AML lesion (c) small RCC lesion (d) large RCC lesion

Note: The sonographic appearance of small AML (<2cms) is hyperechoic with homogeneous echotexture. The sonographic appearance of large AML (>2cms) is hyperechoic with heterogeneous echotexture. The sonographic appearance of small RCC (<2cms) can be hyperechoic, hypoechoic or they may exhibit mixed echogenicity. The sonographic appearance of large RCC (>2cms) is hypoechoic with increasing heterogeneity as they grow in size.

The echogenic characteristics of RCCs are more variable than those of AMLs. RCCs may be hypoechoic or isoechoic relative to normal renal parenchyma. In RCCs cystic area of hemorrhage and tumor vascularity are present. The cellular arrangement was the most important factor for the echogenicity of small RCC and that their hyperechogenicity may be due to the multiple interfaces formed by small spaces between tumor cells. The Ultrasonographic appearance of small RCCs (<2cms) can be hypoechoic means less echogenic and darker than normal kidney tissue, hyperechoic or they may exhibit mixed echogenicity. For large RCCs (>2cms) sonographic appearance is hypoechoic and as they grow become heterogeneous lesions.

1.2 Ultrasound (US)

Numerous imaging modalities like ultrasound, computerized tomography (CT), X-ray, magnetic resonance imaging (MRI) etc. can be used for diagnosing kidney abnormalities but ultrasound is considered to be best for diagnosis of various disorders. In past several years, ultrasonography has become a very popular tool for imaging physiological systems in the body. Widely available ultrasound (US) imaging modality is the first choice for the diagnosis of kidney diseases and it helps in diagnosing the diseases of soft tissue organs such as kidney because of its real-time, inexpensive, non-invasive & non-radioactive properties [3-5]. US imaging modality reliably differentiate solid masses from simple cysts which are most common space occupying lesions in the kidneys. When the returned echoes from the tissues of kidney are exhibited as an image, they form a texture pattern because of the physiognomies of both the imaging system and tissue. This shows that the analysis of US kidney image deals with the interpretation of texture patterns. Texture is an image feature that provides important characteristics for surface and objects identification from the image. Ultrasound measures size and appearance of the kidneys and detect tumors, congenital anomalies, swelling, blockage of urine flow etc. There are many advantages of US such as ultrasound imaging allows faster and more accurate procedures due to its real time capabilities. US is a painless, safe and portable equipment and even better for outer spaces. US give more accuracy than other techniques. One of the main advantage of US is that ultrasound uses high frequency waves to produce moving images onto screen of the inside body including organs, soft tissues, bones etc.

However, the disadvantages of US imaging are artifacts due to the movement of patients and equipment margins. Sonographic appearance of AML and RCC are highly overlapping and sometimes differentiation between these two kidney lesions becomes difficult for the radiologists. Therefore, these glitches limit the clearness of subjective diagnosis. Thus, researchers are showing interest to provide the radiologists with a computer aided diagnosis (CAD) system to assist them in image reading, understanding and decision making [3]. The typical sonographic appearance of the kidney is shown in Figure 1.4.

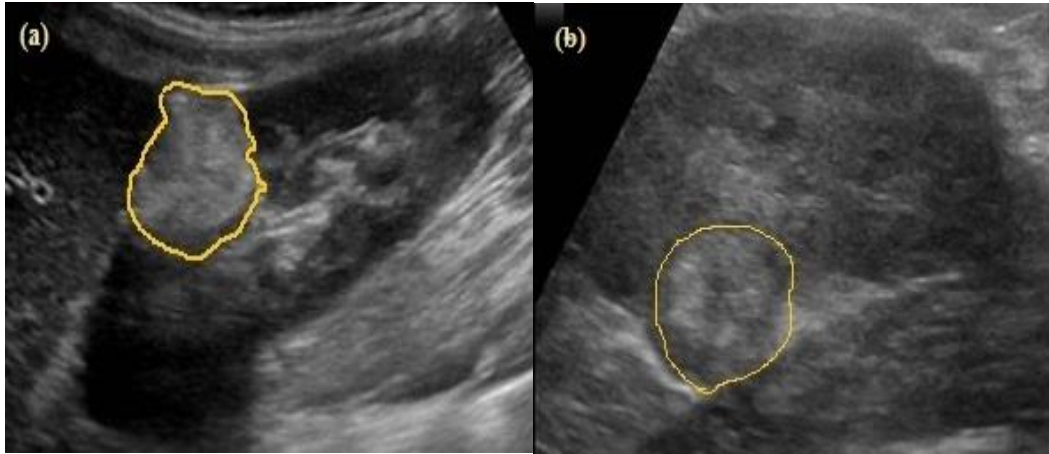


Figure 1.4: B-mode ultrasound kidney images showing different cases. (a) AML image
(b) RCC image

1.3 Need of Computer Aided Diagnosis Systems

With the growth of computer technology, medical image processing algorithms has given abundant opportunity to researchers to investigate the potential of computer-aided diagnostic (CAD) systems for tissue characterization of radiological images. Characterization of tissue indicates the quantitative analysis of tissue imaging features resulting in exact difference between normal and abnormal tissues. So, the outcome of tissue characterization is interpreted by numerical values. The main goal of emerging a computerized tissue characterization system is to provide additional diagnostic information about the underlying tissue which cannot be captured by visual examination of medical images and this information is useful for improving the diagnostic accuracy of sonograms. The discrimination between different tissue echogenicity and texture patterns by visual analysis usually depends upon the experience of radiologists. The participating radiologist opined that, on the basis of echogenicity and low fat tissue, it has become difficult to definitely distinguish between small AMLs and small RCCs. Therefore, a computer aided diagnostic (CAD) system to appropriately recognize and analyze these abnormalities is highly anticipated to help radiologists in medical environment. Therefore, a CAD system for the classification of primary benign and primary malignant focal kidney lesions is tremendously desired to support radiologists during regular medical check-ups.

1.4 Objective of the project work

The main objective of the research work presented in this project report is to enhance the diagnostic potential of ultrasonographic images for identification of different kidney lesions by developing efficient CAD system designs using a representative image database. In order to achieve this, numerous research objectives are formulated according to the needs of the radiologists, based on the practical problems faced by them in routine medical check-ups. These research objectives are described below:

- i. *The collection of a comprehensive and representative image database.*
- ii. *The design, development and implementation of an efficient CAD system for primary benign and primary malignant focal kidney lesions using B-Mode US images.*

The purpose of developing a computerized CAD system is to assist radiologists by providing additional diagnostic information to distinguish between AMLs and RCCs abnormalities which cannot be captured by visual inspection of medical images. When AMLs are less than 2cms, they may confuse with the early stage of RCCs. Therefore, on the basis of echogenicity differentiation between early RCCs and AMLs is difficult. The usefulness of baseline ultrasonography in the hospital is inadequate because it is tough to differentiate these tumors merely on the basis of their echogenicity. So, on visualizing the sonographic appearance of the image, differential diagnosis can be difficult in AML with low fat tissue as it is confused with RCC. In order to overcome these confusions, a decision making CAD system has been proposed which helps the radiologists as a second opinion tool for building balanced opinion on US kidney images and to increase their confidence level in their diagnosis.

Thus for the growth of a fruitful CAD scheme, it is needed not only to develop computer algorithms, but also to examine how much helpful the output of computer would be for radiologists in their diagnosis and how to exploit the effect of the computer output on their diagnosis. With CAD, the final diagnosis is made by the radiologist.

CHAPTER 2

LITERATURE REVIEW

2.1 Introduction

Recently, one of the leading research topics in medical imaging and diagnostic radiology is a CAD system. The rudimentary idea of CAD is to provide a computer output to assist radiologists and other health care experts in reading and understanding the image and to differentiate between various anomalies. With CAD, the final diagnosis is made by the radiologist. Numerous kind of CAD systems are advanced for the detection and classification of various lesions in medical imaging, including X- rays, MRI, CT, and US [3]. The organs presently being subjected for the research of CAD contains the breast, chest, liver, kidney and the vascular and skeletal systems. It can be noticed that past CAD implementations does not include kidney lesions.

The research works described in allied studies have proposed several CAD system designs for kidney classification. The brief depiction of related studies is shown below in table 2.1.

2.2 Different CAD System Designs for the Classification of Kidney US images

For the characterization of B- mode kidney ultrasound images, very rare studies have been presented in literature.

Table 2.1: Explanation of related studies carried out for kidney image classification.

Authors	Dataset Description			
	Kidney image classes	AOI size	No. of images	Features Extracted
Raja et al [3]	Nor, MRD, Cyst	SKT	150	Statistical, MI, Power spectral and Gabor
Raja et al [4]	Nor, MRD, Cyst	SKT	150	Gabor wavelet
Raja et al [5]	Nor, MRD, Cyst	SKT	150	Power spectral
Jose et al [6]	Nor, MRD, Cyst	SKT	35	Histogram ,GLCM and SGLDM
Akkasaligar et al [7]	Nor and Cyst	SKT	52	GLCM and GLRLM
Subramanya et al [8]	Nor, MRD, Cyst	32×32	35	FOS, MI, GLCM, GLRLM and Laws' mask

Raja et al [9]	Nor, MRD, Cyst	SKT	150	Statistical, MI and Power spectral
Raja et al [10]	Nor, MRD, Cyst	SKT	150	Statistical and MI

Note: AOI: Area of interest, MI: Moment invariant features, FOS: First order statistics features, GLCM: Gray length co-occurrence matrix features, GLRLM: Gray level run length matrix features, SGLDM: Spatial gray level dependence matrix features, Nor: Normal, MRD: Medical renal diseases, SKT: Segmented kidney tissue

The study in [3] proposed an approach for automatic judgment and classification of kidney ultrasound images into Normal (Nor), medical renal disease (MRD) and cyst with statistical, algebraic moment invariant (MI), power spectral and Gabor features. For each kidney US image, total 36 features are extracted by using various kinds of conclusion support classifiers named as hybrid fuzzy-neural network system and enhanced multi-layer back propagation network. It has been concluded that the hybrid fuzzy neural network gives the best performance than the enhanced multi-layer back propagation system.

The study in [4] reported classification of three classes namely, Nor, MRD and Cyst are considered for the analysis of dominant Gabor wavelet features by using k-nearest neighbours (kNN) classifier and these features gives the classification accuracy of 86.6% for Nor, 76.6% for MRD and 83.3% for Cyst.

The study in [5] reported classification of three kidney classes namely, Nor, MRD and Cyst are considered for the analysis of power spectral features such as P_T^{W1} ; P_T^{W2} ; P_{T-W12}^{R1} ; P_{T-W12}^{R2} ; P_{T-W1d}^{R3} and P_{T-W1d}^{R4} features. The results obtained show that the features are highly content descriptive and provide discrete range of values for each kidney category. Such isolated feature values enable to identify the kidney categories objectively which may be used as a secondary observer.

The study in [6] proposed an approach to implement a computer-aided decision support system for an automated diagnosis and classification of kidney images into Nor, MRD and Cyst with fractal features, histogram-based features like mean, variance, skewness, kurtosis, energy, and entropy, first order gray level statistical features like mean, dispersion, variance,

average energy, skewness, kurtosis, median and mode and spatial gray level dependence matrix (SGLDM) feature. In this study Bayesian Classifier is used for classification task.

The study in [7] proposed an approach in which the acquired images are manually cropped to find the area of interest (AOI) of kidney. The cropped images are pre-processed using three different filters namely Gaussian low-pass filter, median filter and Weiner filter to remove speckle noise. In this study two kidney classes namely, Nor and Cyst are considered for the analysis of texture features by using gray level co-occurrence matrix (GLCM) and run length matrix (RLM) features and kNN classifier is used for classification task.

The study in [8] reported the classification of Nor, MRD and Cyst classes with texture analysis methods. The images were pre-processed to extract 32×32 size AOIs from each image. Statistical features like first-order statistics (FOS) features, gradient based features, MI, GLCM, RLM and law features has been extracted from these AOIs s by using support vector machine (SVM) classifier. Depending on the overall classification accuracy (OCA), only some feature sets are considered for the classification task such as differential evolution feature selection (DEFS).

The study in [9] reported classification of Nor, MRD and Cyst with statistical texture analysis methods such as first-order statistics (FOS), MI, power spectral features to identify and classify the kidney disorders with ultrasound scan. In this study 28 features are extracted. Artificial neural network (ANN) classifier is used for the classification task. This study achieves the OCA of 90.4% for Nor, 86.6% for MRD and 85.7% for Cyst.

The study in [10] reported the analysis of abdominal ultrasound kidney images to evaluate the tissue characteristic for implementing unbiased diagnosis procedure and to classify important kidney orders. In this study three kidney classes namely, Nor, MRD and Cyst are considered for the analysis of statistical texture analysis methods and MI features. In this study 15 features are extracted out of which 6 features are highly significant.

2.3 Concluding Remarks

From the above studies, it can be observed that the related studies for classification of renal diseases using ultrasound images are few and most of the work in recent years on these studies have considered three kidney image classes, viz. Normal (Nor), Medical Renal Disease (MRD) and Cyst [3-6, 8-10]. From these studies, it is also seen that, only two research works carried out in study [7, 8] proposed the CAD systems based on the extraction of AOIs from the kidney. A CAD system for classification of primary benign and primary malignant focal kidney lesions has not been developed till date in the research area, therefore, this task has been carried out in the present work.

CHAPTER 3

METHODOLOGY

3.1 Introduction

From the extensive literature survey presented in the previous chapter, it is observed that maximum related studies carried out in the past are based on three classes of kidney, viz. Normal (Nor), Medical Renal Disease (MRD) and Cyst, while very rare studies has shown the CAD systems based on AOIs extracted from the kidney [7, 8] and a CAD system for classification of focal kidney lesions has not been established till date. Thus in the current work, taking into account the effect of AOI size and location on performance of the algorithms, a CAD system design is proposed for the classification of different kidney lesions on the basis of their underlying texture characteristics derived from the kidney US images. In this work, two different kidney classes, viz. Primary benign (AML) and Primary malignant (RCC) kidney lesions has been taken so as to distinguish between small AMLs (<2cms) and small RCCs (<2cms) and for the class separability task, various classifiers have been used. The incentive behind considering these two kidney image classes is that the occurrence of these focal lesions is more in comparison to other primary benign and malignant kidney lesions. Amongst various benign lesions, AML is one of the utmost commonly occurring primary benign lesion and among several malignant lesions RCC is considered as the most frequently occurring primary malignant lesion.

3.2 General CAD System Design

The term CAD refers to the use of computers to assist doctors in objective diagnosis. The main objective for developing such CAD system is to, provide opportunities such as a measurable worldwide reference for the US kidney images, implement image recovery in various medical application systems, make a computerized tissue characterization system that automatically identifies the pathology and make relative study on images for taking final decisions [3-5] [9, 10]. Recently, CAD has become one of the major research subjects in medical imaging and diagnostic radiology. So, for the development of a fruitful CAD system design it is essential not only to develop

algorithms of computer, but also to investigate how much constructive the output of computer would be for radiologists and medical experts in their diagnosis, how to measure the benefits of the computer output for radiologists, and how to capitalize the result of the computer output on their diagnosis.

In the present work, numerous CAD systems have been proposed for the classification of AML and RCC lesions on the basis of their underlying texture characteristics using B-Mode kidney US images.

A general framework of a CAD scheme is depicted in Figure 3.1 and each module of CAD system is explained below. The AOI extraction module is described in section 3.2.2. The feature extraction module is described in detail in section 3.2.3. A wide variety of classifiers are used for the classification purpose is described in section 3.2.4. The main classifier used to carry out the present research work is described in section 3.2.4.3.

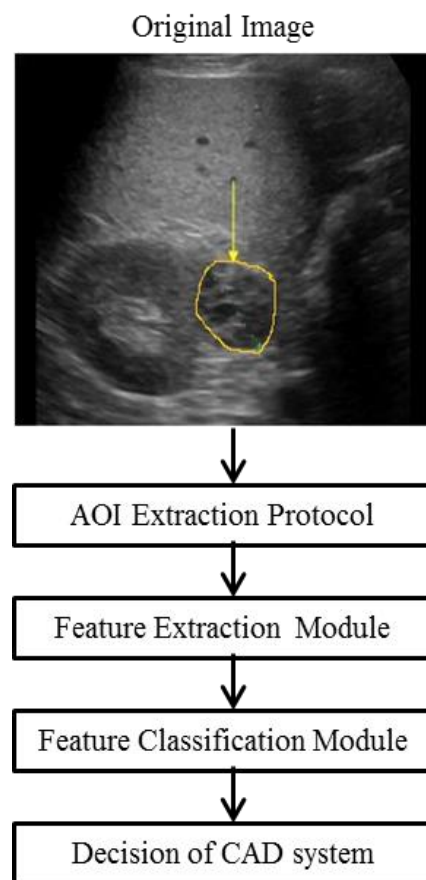


Figure 3.1: General framework of a CAD system design

3.2.1 Dataset Collection and Description

In order to test the CAD system, a publically obtainable benchmark database has been used and is available for the research purpose online [11]. The images in the database are classified into two types namely, AML and RCC. Each image in the database is of size 300×225 pixels having 96 dpi horizontal and vertical resolutions with a gray scale comprising of 256 tones. The digital images are acquired from Aloka ultrasound scanning system and Hitachi high end ultrasound systems.

3.2.2 Area of Interest (AOI) Selection Protocol

For calculating various texture features, the size of Area of Interest (AOI) has been selected wisely from the region well within the boundary of each lesion in such a manner that it must deliver a good statistical population for making the correct decisions in CAD system [12, 13]. In earlier studies, it has been stated by many researchers that to provide good sampling distribution for estimating reliable statistics AOI size must be at least 800 pixels [13]. Different sizes of AOI that have been selected in the literature for the classification are 32×32 [8] [13], 30×30 [14], 60×60 [15], 10×10 [16-17], 40×40 [18], 50×50 [19]. In this work, multiple non-overlapping fixed size AOIs of 32×32 and single AOI of variable sizes are extracted manually from inside the lesions so as to get the better results. The participating radiologist suggested that, AOIs should be taken from inside the lesions avoiding the renal sinus region which consists of fats, kidney blood vessels etc. The fact of selecting the small AOI size of 32×32 is that greater numbers of samples are attained and time taken for the calculation of features is least in comparison to bigger sized AOIs. The fact for variable sizes AOIs is that depending on the size of lesions, the largest rectangular AOI has been cropped from the region inside the lesion. The participating radiologist opined that the shape or margin features are not important for differential diagnosis between focal kidney lesions. Therefore another attempt has been made to take the largest AOI from each lesion leaving the boundary of the lesion so as to compute reliable estimates of texture features. The selection and extraction of AOIs from focal kidney lesion is shown in Figure 3.2.

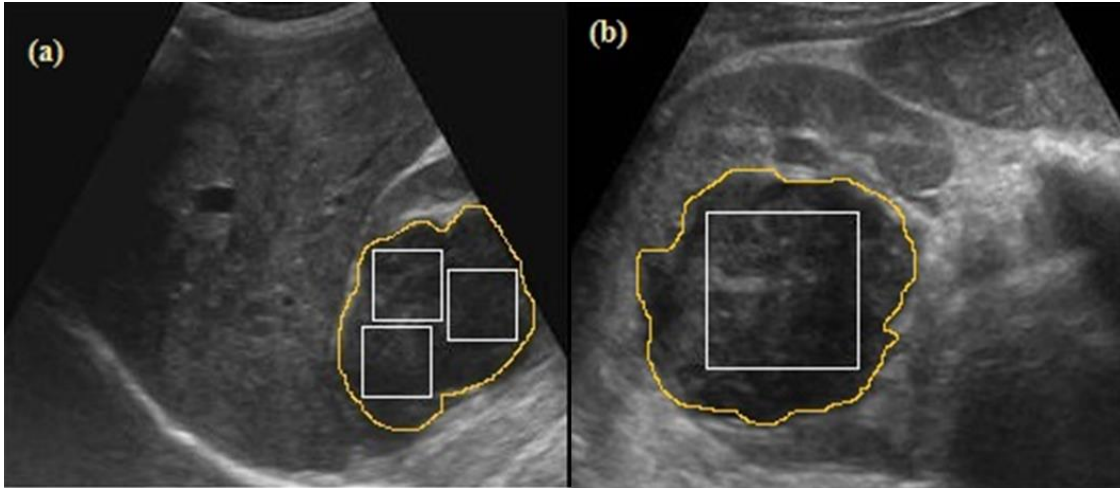


Figure 3.2: Sample AOI images. (a) Fixed size AOI image (b) Variable size AOI image

3.2.3 Feature Extraction Module

The key idea behind extraction of features is to calculate the mathematical descriptors describing the properties of AOI. These mathematical descriptors are further classified as shape based features (morphological features) and texture based features (intensity distribution based features) [20, 21]. The radiologist opined that for kidney lesions only texture based features gives the sufficient amount of information and shape based features do not provide any significant information for differential diagnosis between AML and RCC lesions. Therefore, the proposed CAD system design is made on the basis of textural features only. There are a various methods to extract the texture features including statistical, spectral and spatial filtering based methods. From the comprehensive evaluation of the related studies on classification of kidney US images [3-10, 22-27], it can be observed that all these texture features are important for the classification of focal kidney lesions also. Accordingly, for the present task of classification between AML and RCC lesions, the texture features are extracted for each AOI image using statistical, spectral and spatial filtering based methods as shown in Figure 3.3. The description of these three texture based methods is shown below in section 3.2.3.1, 3.2.3.2 and 3.2.3.3.

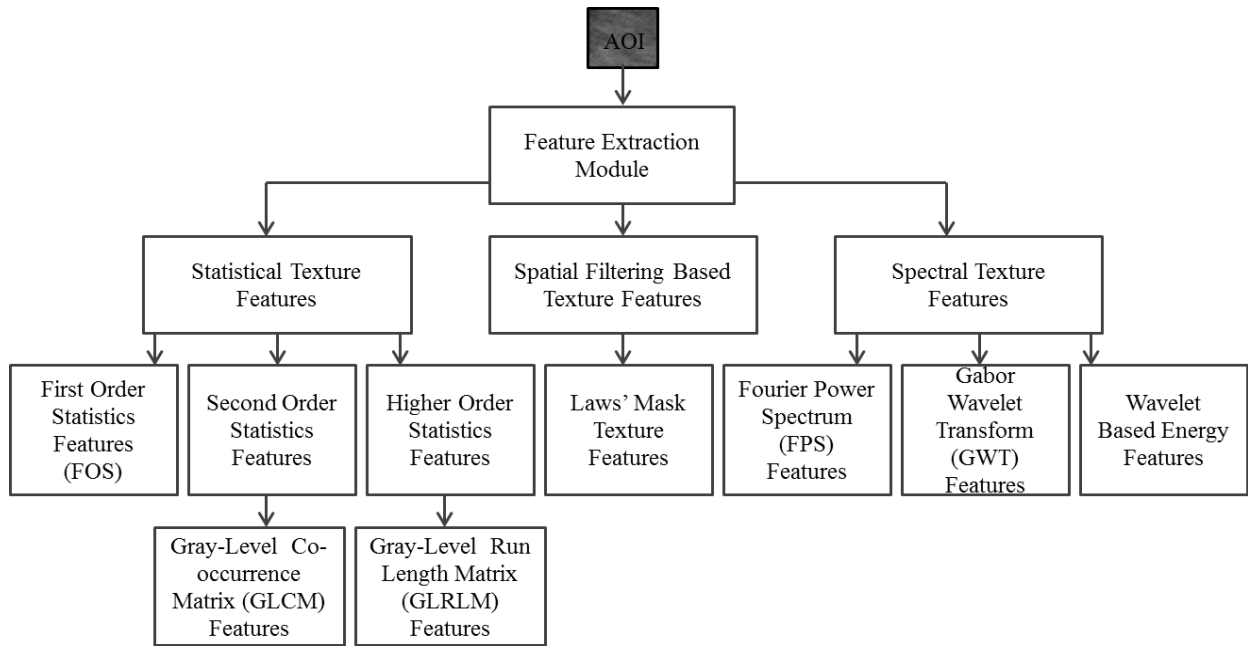


Figure 3.3: Texture features computed for each ROI image.

3.2.3.1 Statistical Texture Features

The statistical methods are used to excerpt the texture features based on spatial distribution of the gray level intensity values in image. Based on the number of pixels used to compute the texture features, statistical methods can be classified into first-order statistics, second-order statistics and higher-order statistics methods.

3.2.3.1.1 First Order Statistics Features (FOS)

The first order statistics are derived from the gray level intensity histograms of the image. For each AOI, six FOS texture features i.e. average gray level, smoothness, standard deviation, third moment, uniformity and entropy are calculated [8, 18 23,27].

3.2.3.1.2 Second Order Statistics Features (GLCM)

Second order statistics comprises the calculations with the Gray level co-occurrence matrix (GLCM). GLCM tells how frequent combinations of pixels pairs having different gray level occurs in an image having separation of different dimensions in different directions say 0° , 45° , 90° , 135° . Total thirteen GLCM features are calculated from each AOI i.e. variance, sum average, angular second moment, contrast, correlation, inverse difference moment, sum variance, difference variance, sum entropy, entropy,

difference entropy, information measures of correlation-1 and information measures of correlation-2 [13,23,27-29].

3.2.3.1.3 Higher Order Statistics Features (GLRLM)

Gray level run length matrix (GLRLM) features are used to calculate the higher order statistics. By using different combinations of intensities texture features are calculated. Gray level run is made up of the set of successive pixels of gray levels and the run length (means the number of times a run occurs). Total eleven GLRLM features are calculated from each AOI i.e. short run emphasis (SRE), long run emphasis (LRE), short run low gray level emphasis (SRLGLE), short run high gray level emphasis (SRHGLE), long run low gray level emphasis (LRLGLE), low gray level run emphasis (LGLRE), high gray level run emphasis (HGLRE), long run high gray level emphasis (LRHGLE), gray level non uniformity (GLN), run percentage (RP) and run length non-uniformity (RLN) [23, 27, 32-35].

3.2.3.1.4 Other Statistical Features

(a) Edge Features (Absolute Gradient): More information about texture is always present at the edges. In order to measure the spatial variation of gray levels across an image, gradient of an image is used. Gray level changes abruptly at an edge. If there is no abrupt change in gray level then gradient will be low otherwise it will be high. Two texture features, i.e. absolute gradient variance and absolute gradient mean are computed in edge features [36].

(b) Neighborhood Gray Tone Difference Matrix Features: Neighborhood Gray Tone Difference Matrix (NGTDM) features reflect a grayscale difference. With the neighbouring pixels and with a definite gray scale, NGTDM imitates a grayscale difference between pixels. Five NGTDM features are calculated such as complexity, coarseness, contrast, strength and busyness [37, 38].

(c) Statistical Feature Matrix: Statistical Feature Matrix (SFM) calculates the statistical properties of pixels such as (1) the matrix size is dependent on the maximum distance used instead of the number of gray-levels and (2) the matrix can be extended very easily

at different distances. SFM computes four features namely periodicity, coarseness, roughness and contrast.

(d) *Gray Level Difference Statistics*: On the basis of co-occurrence of a pixel pair having a certain absolute difference in gray-levels, five Gray Level Difference Statistics (GLDS) features are extracted such as homogeneity, energy, contrast, entropy and mean [39, 40].

3.2.3.2 Spatial Filtering Based Texture Features (Signal Processing based Methods)

Laws' Mask Texture Analysis: The Laws' texture features are spatial filtering based texture descriptors which convolution masks are used as filters and AOIs are convolved with these special filters so that the underlying texture characteristics are improved. These filters perform local averaging (L), spot detection (S), wave detection (W), edge detection (E) and ripple detection (R), so as to determine the properties of the texture [23, 27, 28, 41]. Laws' masks features can be calculated by using special 1-D filters of lengths 3, 5, 7 and 9 which are used to compute five statistical parameters i.e. mean standard deviation, skewness, kurtosis and entropy from each AOI. In law 3 and 7, total 30 features are obtained for each AOI and in law 5 and 9, total 75 features are obtained for each AOI. The description of Laws' mask texture features is shown in Table 3.1

Table 3.1: Description of Laws' masks of different lengths.

Length of 1-D filter	1-D filter coefficients	No. of 2D Laws' masks	No. of TR images
3	L3=[1, 2, 1] E3=[-1, 0, 1] S3=[-1, 2, -1]	9	6
5	L5= [1, 4, 6, 4, 1] E5= [-1, -2, 0, 2, 1] S5= [-1, 0, 2, 0, -1] W5= [-1, 2, 0, -2 1] R5= [1, -4, 6, -4, 1]	25	15
7	L7= [1, 6, 15, 20, 15, 6, 1] E7= [-1 -4, -5, 0, 5, 4, 1] S7= [-1, -2, 1, 4, 1, -2, -1]	9	6
9	L9= [1, 8, 28, 56, 70, 56, 28, 8, 1] E9= [1, 4, 4, -4, -10, -4, 4, 4, 1] S9= [1, 0, -4, 0, 6, 0, -4, 0, 1] W9= [1, -4, 4, -4, -10, 4, 4, -4, 1] R9= [1, -8, 28, -56, 70, -56, 28, -8, 1]	25	15

Note: TR: rotation invariant texture images

3.2.3.3 Spectral Texture Features (Transform Domain based Methods)

Feature extraction can also be done in the transform domain over various scales by using different multiresolution schemes like discrete wavelet transform (DWT), Gabor wavelet transform (GWT) and wavelet packet transform (WPT). It is logical to compute texture features in the transform domain as human visual system processes images in a multiscale way and scale is considered to be an important aspect for analysis of texture [24].

3.2.3.3.1 Two-Dimensional Gabor Wavelet Transform (GWT) Features

The two dimensional Gabor Wavelet Transform (2D-GWT) provides useful texture descriptors by using multi-scale features assessed at different scales and orientations. The 2D-GWT, considering three scales (0, 1, 2) and seven orientations (22.5°, 45°, 67.5°, 90°, 112.5°, 135°, 157.5°), result in a group of (7 × 3) 21 wavelets. When this cluster of Gabor filters family of 21 wavelets is convolved with the AOI image, a set of 21 feature images are attained. Every filtered image represents the information of image at a certain scale and orientation [42, 43]. From these 21 feature images, two statistical features such as mean and standard deviation are calculated as texture descriptors resulting in (21 feature images × 2 statistical parameters) 42 features for each AOI [21, 42, 43]. The real part of Gabor filter family of 21 feature images resulting from a 13 × 13 convolution mask with 3 scales and 7 orientations are shown in Figure 3.4.

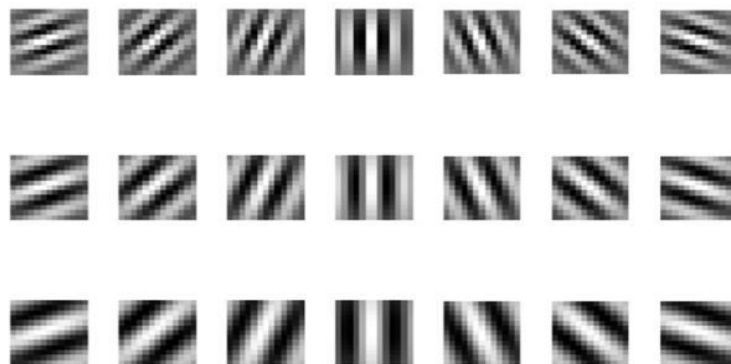


Figure 3.4: Gabor filters family of 21 wavelets (images) acquired for a sample AML ROI image with scales (0, 1, 2) from top to bottom and orientations (22.7°, 45°, 67.5°, 90°, 112.5°, 135°, 157.5°) from left to right.

3.2.3.3.2 Fourier Power Spectrum Features

For each AOI, two spectral features i.e. radial sum and angular sum has been calculated by using the discrete Fourier transform (i.e., DFT) [27, 33].

3.2.3.3.3 2-Dimensional Discrete Wavelet Transform (DWT) Features

A two-dimensional Discrete Wavelet Transform (2D- DWT) when applied to images can be seen as 2 one-dimensional (1-D) transform functions applied to rows and columns of the image separately [44, 45]. When this process is applied to an AOI image and decomposition is done upto 2nd level, 1 approximate sub image A_j and 6 orientation selective detailed sub images $D_j^{(k)}$, $k = h, v, d$ are generated. Normalized energy is computed as a texture measure from each sub image. This wavelet depiction of an image is shown in Figure 3.5.

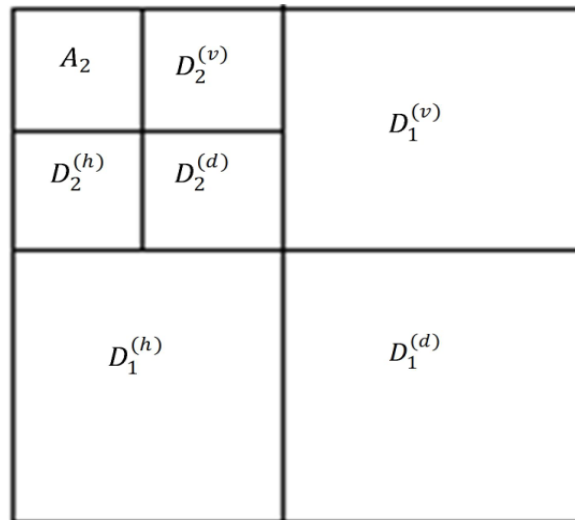


Figure 3.5 Wavelet depiction of image up to 2nd level of decomposition.

For feature extraction, the wavelet filter choice is based on some possessions which are important for texture description [13, 42]. For selecting an appropriate wavelet filter, the properties such as support width, shift invariance, orthogonality or biorthogonality and symmetry are considered. Wavelet filters that deliver compact support are needed due to their easiness of implementation. Orthogonality property is obligatory at each level of decomposition for energy conservation. Symmetry is also another important property which is required to evade any dephasing while processing images. On the basis of these properties, wavelet filters like Haar (db1), Daubechies (db4 and db6), Coiflets (coif1

and coif2), Biorthogonal (bior3.1, bior3.3 and bior4.4) and Symlets (sym3 and sym 5) are considered for analysis. The properties of these filters are summarized in Table 3.2.

Table 3.2: Properties of wavelet filters used

Wavelet Filter	Biorthogonal	Orthogonal	Symmetry	Asymmetry	Near Symmetry	Compact Support
Db	No	Yes	No	Yes	No	Yes
Haar	No	Yes	Yes	No	No	Yes
Bior	Yes	No	Yes	No	No	Yes
Coif	No	Yes	No	No	Yes	Yes
Sym	No	Yes	No	No	Yes	Yes

3.2.4 Classification Module

The classification procedure examines the numerical properties of numerous image features and labels the data into different classes. To predict the class membership of indefinite data and unknown data instances based on the training set of data containing instances whose class membership is known, machine learning techniques (i.e. various classifiers) are used. The main job of a classifier is to allot a given sample to its concerned class. In this classification section different classifiers such as kNN, PNN and SVM are employed to classify the unknown testing cases of kidney ultrasound images of different classes based on the training instances. In order to evade any bias induced by unbalanced feature values, the extracted features are normalized in the range [0, 1] by using minima-maxima normalization procedure.

3.2.4.1 *k*-Nearest Neighbors (*k*NN) Classifier

The *k* nearest neighbor (*k*NN) classifier is based on the idea of guesstimating the class of an unknown instance from its neighbors. The *k*NN is a type of instance based machine learning algorithm in which the best number of *k* neighbors and the best feature space transformation is selected. It tries to bunch the instances of feature vector into disjoint classes with a supposition that instances of feature vector lying near to each other in feature space represent instances belonging to the same class. The class of an unknown instance in testing dataset is selected to be the class of majority of instances

among its k-nearest neighbours in the training dataset. The benefit of kNN is its capability to deal with multiple class difficulties and is robust to noisy data as it averages the k- nearest neighbours [27, 46-48]. Euclidean distance is used as a distance metric. The classification performance of kNN classifier depends on the value of k. In the present study, the best values of k and number of principal components (PCs) to be taken is determined by executing recurring experiments for the values of $k \in \{1, 2, \dots, 9, 10\}$ and number of PCs $\in \{1, 2, \dots, 14, 15\}$. If same accuracy is attained for more than one value of k then smallest value of k is used to obtain the result.

3.2.4.2 Probabilistic Neural Network (PNN) Classifier

The Probabilistic Neural Network (PNN) is a supervised feed-forward neural network or a statistical algorithm, used for assessing the probability of class membership [27, 49-52]. A PNN classifier mainly maps any input pattern into a number of classifications. The design of PNN contains four layers: input layer, pattern layer, summation layer and output layer. In the input unit, primitive values are passed to the 'n' neurons and those values from the input unit are further passed to the hidden units in the pattern layer where responses for each unit are calculated. In the pattern layer, there are 'k' numbers of neurons, one for each class and a probability density function for each class is defined on the basis of training dataset and optimized kernel width parameter. In the summation layer, values of each hidden unit are summed to get response in each category. Maximum response is taken from all categories in the output layer i.e. a decision layer, to get the class of the unknown instance. The ideal choice of spread parameter (SP) i.e. the kernel width parameter is critical for the classification. In the present work, the best values used for SP and optimal number of PCs to design a PNN classifier are determined by executing repeated tests for the values of $SP \in \{1, 2, \dots, 9, 10\}$ and number of PCs $\in \{1, 2, \dots, 14, 15\}$.

3.2.4.3 Support Vector Machine (SVM) Classifier

The Support Vector Machine (SVM) classifier refers to a class of supervised machine learning algorithms because the classes are already defined for the training sets. SVM is also called as Support Vector Network and is mainly a method that performs

classification tasks by building hyper planes in a multidimensional space that splits cases of different class labels. SVM supports both regression and classification tasks and can hold many continuous and categorical variables. SVM classifier is based on the idea of decision planes that describe decision boundary. This classifier is operative in high dimensional spaces and is also effective in those cases where number of dimensions is larger than the number of samples. In SVM classifier, non-linear training data from input space is mapped to higher dimensional feature space by using kernel functions. Kernel based SVM is a best classifier for the class separability with very less no. of errors. Kernels such as polynomial kernel, sigmoid kernel and Gaussian radial basis kernel function are the most frequently used kernels. For the present study, SVM classifier is implemented using LibSVM library [53] and the performance of Gaussian radial basis function kernel is studied for the present study. A good generalization performance is acquired by right choice of the kernel parameter γ and regularization parameter C and the best values of C and γ has been obtained using grid search procedure. The regularization parameter C keeps low training error value and tries to maximize the margin, while the kernel parameter γ chooses the curvature of decision boundary. In the present work, for each combination of (C, γ) , ten-fold cross validation is done on the training data such that $C \in \{2^{-4}, 2^{-3} \dots 2^{15}\}$ and $\gamma \in \{2^{-12}, 2^{-11} \dots 2^4\}$. The ideal values of regularization parameter and kernel parameter can be attained by this net search process in the parameter space for which the training accuracy is maximum. Hence, the selection of kernel parameter γ and regularization parameter C is very important for better performance of the classifier [8, 13, 22, 23, 27, 43, 54-72].

3.2.4.4 Classifier performance evaluation criteria:

The performance of CAD system for the classification of focal kidney lesions can be measured by two main parameters namely overall classification accuracy (OCA) and individual class accuracy (ICA). Calculations of OCA and ICA are done by using the confusion matrix (CM).

$$\text{OCA} = \frac{\Sigma \text{ No. of correctly classified images of each class}}{\text{Total images in testing dataset}}$$

$$\text{ICA} = \frac{\text{No. of correctly classified images of one class}}{\text{Total no. of images in the testing dataset for that class}}$$

3.3 Concluding Remarks

After carrying out extensive literature survey, it was observed that various CAD system designs have proven useful to the radiologists in routine medical practice as second opinion tools for kidney tissue classification in cases where a clear discrimination cannot be made subjectively between the different lesions. In light of this fact, CAD system design employing the texture analysis techniques of feature extraction and feature classification have been proposed in the present work for two-class kidney tissue classification. Feature extraction is done using statistical, spatial filtering based and spectral methods and finally classification performance of each texture feature is evaluated using different classifiers.

A detailed description of each proposed CAD system design is given in the upcoming chapters.

CHAPTER 4

CAD SYSTEM DESIGN FOR CLASSIFICATION OF FOCAL KIDNEY LESIONS USING GABOR WAVELET TEXTURE FEATURES

4.1 Introduction

The objective of the present study is to develop a CAD system design for the differential diagnosis between AML (i.e., primary benign focal kidney lesion) and RCC (i.e., primary malignant focal kidney lesion). The incentive behind considering these kidney image classes is that the occurrence of these focal lesions is very high in comparison to other primary benign and primary malignant lesions. The differentiation between other focal lesions like cysts, metastasis is easy due to the typical sonographic appearance of the former one, but differential diagnosis between small AMLs (<2cms) and small RCCs (<2cms) lesions is difficult even for the experienced radiologists. The discrimination between different tissue echogenicity and texture patterns by visual analysis usually depends upon the experience of radiologists. The participating radiologist opined that, on the basis of echogenicity and low fat tissue, it has become difficult to clearly distinguish between small AMLs and small RCCs lesions. So, it is very important to overcome these limitations by design of an efficient CAD system. Therefore, a CAD system to correctly identify and analyze these abnormalities is highly anticipated to help radiologists in medical environment.

In light of this fact, a CAD system design is proposed in this chapter for the characterization of primary benign and primary malignant focal kidney lesions by using Gabor wavelet texture features and a support vector machine (SVM) classifier has been used for the classification task.

4.2 Proposed CAD System Design

In the present work, the CAD system has been proposed for the classification of AML and RCC lesions using B-Mode kidney US images. The block diagram of the proposed CAD system design is shown in Figure 4.1

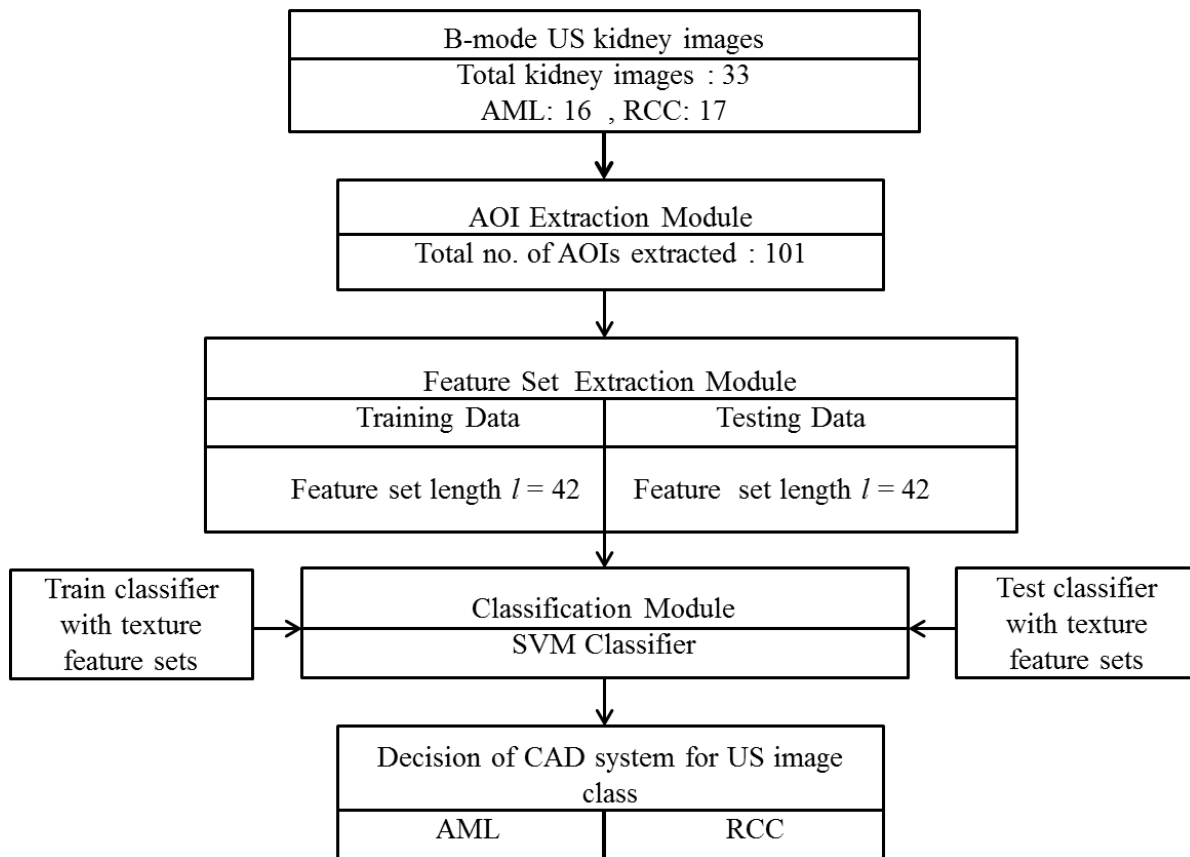


Figure 4.1: Proposed CAD system design.

The objective of developing a computerized tissue characterization system is to assist radiologists by providing additional diagnostic information to distinguish between AMLs and RCCs abnormalities which cannot be captured by visual examination of medical images. When AMLs are small, they may be confused with the early stage of RCCs. Therefore, differentiation between early RCCs and AMLs is difficult. The usefulness of baseline ultrasonography in the hospital is inadequate because it is tough to differentiate these tumors merely on the basis of their echogenicity. So, on visualizing the sonographic appearance of the image, differential diagnosis can be difficult in AML with low fat tissue as it is confused with RCC. In order to overcome these confusions, a decision making CAD system has been proposed which helps the radiologists as a second opinion tool for building balanced opinion on US kidney images and to increase their confidence level in their diagnosis.

The CAD system helps the ultrasound technicians in identifying the infected areas which might be missed by them during the ultrasonography. In some cases, the

confidence of radiologists is less in their diagnosis, in that case it is estimated that the final results can be amended by use of the computer output. The overall effect of final diagnosis depends upon the performance level of the computer. Basically, the CAD system consists of AOI extraction, feature extraction and classification module. The description of these modules is shown in below sections.

4.2.1 Dataset Description Module

In the present work, benchmark database of 33 B-mode kidney US images consisting of 16 AML images with solitary AML lesions and 17 RCC images have been used. The digital images are acquired from Aloka ultrasound scanning system and Hitachi high end ultrasound systems. Each image in the database is of size 300×225 with a grey scale consisting of 256 tones and horizontal and vertical resolution of 96 dpi.

4.2.2 AOI Extraction Module

For the texture measurements, the size of Area of Interest (AOI) is selected carefully, considering the fact that it should provide a virtuous statistical population. For executing the CAD system design, 101 AOIs are extracted from 33 images of database having 23 AML AOIs (from 16 AML kidney images) and 78 RCC AOIs (from 17 RCC images). In AOI extraction module, from each ultrasonographic image, multiple non overlapping fixed size AOIs of size 32×32 are extracted. *Multiple AOIs* has been taken from inside the lesion of kidney depending on the size of the lesion. In this study, AOIs are manually extracted from B-mode kidney US images.

The selection and extraction of AOIs from focal kidney lesion is shown in Figure 4.2.

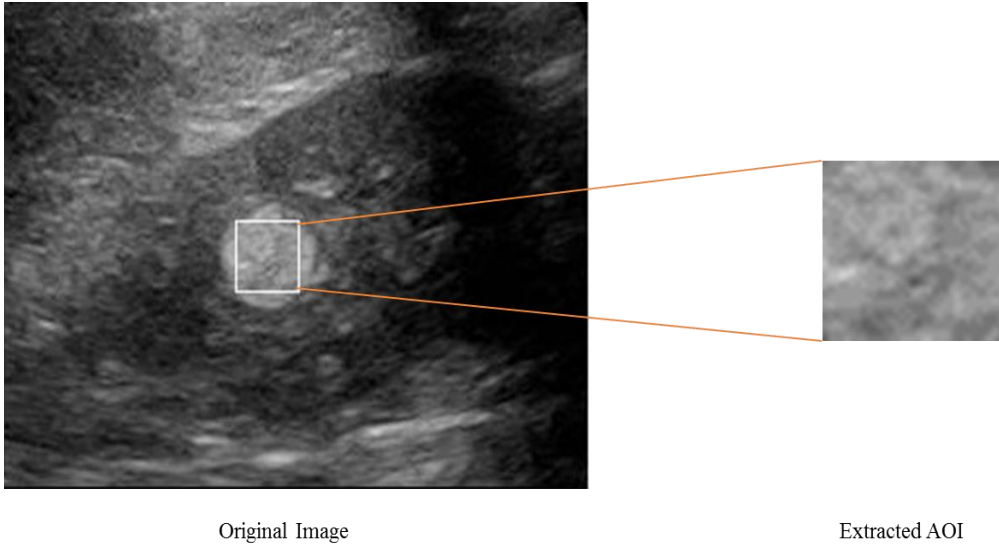


Figure 4.2: Sonographic image of a small AML with marked AOI.

The distribution of the acquired database with 33 B-mode kidney US images among AML and RCC image categories and the division of AOIs in training and testing data set is depicted in Table 4.1.

Table 4.1: Dataset description for two class classification

B- mode US kidney images (33)				
Total AOIs: 101				
Image Classes	No. of images	No. of AOIs	AOIs in training set	AOIs in testing set
AML	16	23	12	11
RCC	17	78	39	39

4.2.3 Feature Extraction Module

Feature extraction module is used to calculate the texture based features for understanding the underlying textural properties of AOI images. In the present work, visual and non-visual echotexture features are computed by using transform domain feature extraction method i.e. Gabor Wavelet Transform (GWT) method. In this method, the statistical features such as mean and standard deviation are computed for

each ROI from 21 feature images (3 scales and 7 orientations) resulting in 42 features. Set of Gabor features is shown in Figure 4.3.

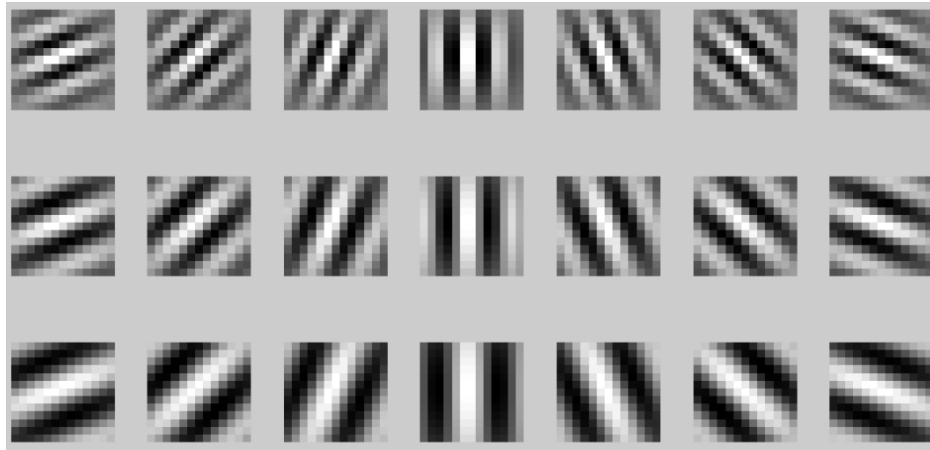


Figure 4.3: Gabor filters family of 21 wavelets (images) acquired for a sample AML ROI image with scales (0, 1, 2) from top to bottom and orientations (22.7° , 45° , 67.5° , 90° , 112.5° , 135° , 157.5°) from left to right.

4.3 Results and Discussion

For evaluating the performance of the proposed CAD system design, rigorous experimentation has been carried out in the present work to distinguish the ultrasound images of different kidney lesions using SVM classifier on the basis of features extracted by using GWT method.

The performance of the CAD system design has been compared with respect to overall classification accuracy (OCA), individual class accuracy (ICA), and the computational efficiency.

4.3.1 *To obtain the classification performance of spectral features for primary benign (AML) and primary malignant (RCC) Kidney lesions using SVM classifier.*

In this experiment, a kernel based SVM classifier is used to obtain the classification performance of Gabor wavelet transform features. The results of experiment are shown in Table 4.2.

Table 4.2: Classification performance of spectral features using SVM classifier for two-class classification.

Classifier	CM			OCA (%)	ICA _{AML} (%)	ICA _{RCC} (%)
		AML	RCC			
SVM		AML	RCC	90.0	63.6	97.4
	AML	7	4			
	RCC	1	38			

Note: CM: Confusion matrix, AML: Angiomyolipoma class, RCC: Renal Cell Carcinoma class, OCA: Overall classification accuracy, ICA_{AML}: Individual class accuracy for angiomyolipoma, ICA_{RCC}: Individual class accuracy for renal cell carcinoma.

From the table 4.2, it can be observed that, for GWT features the overall classification accuracy (OCA) of 90.0 % is attained by using SVM classifier. Out of total 50 testing instances, 45 instances (45/50) are correctly classified and 5 instances (5/50) are misclassified. It can also be observed that the individual class accuracy (ICA) for AML is 63.6 % and for RCC it is 97.4 %.

4.4. Concluding Remarks

A study on the classification of kidney lesions has been carried out. Texture features namely Gabor wavelet transform features are calculated for the classification of kidney tissue and also for capturing the textural variations of benign and malignant kidney lesions. In primary benign and primary malignant focal lesions, region of interest is taken from inside the lesions.

It can be observed from the rigorous experimentation that, for two-class characterization of kidney tissue, the SVM based CAD system gives the highest OCA of 90.0 % for AML and RCC lesions. It can be concluded that transform domain based features are important to account for the textural variations shown by the primary focal lesions.

The obtained results of proposed CAD system design specify their usefulness to support radiologists for the differential diagnosis of AML and RCC lesions during routine medical practice.

CHAPTER 5

CAD SYSTEM DESIGN FOR CHARACTERIZATION OF FOCAL KIDNEY LESIONS USING STATISTICAL AND SPECTRAL TEXTURE FEATURES

5.1 Introduction

The aim of the present study is to develop a SVM based CAD system for the characterization of focal kidney lesions from B-mode ultrasound images. Angiomyolipoma (AML) is a most commonly occurring primary benign lesion and renal cell carcinoma (RCC) is one of the most commonly occurring primary malignant lesion of kidney. Characterization of benign and malignant focal kidney lesions such as AMLs and RCCs from ultrasound images is an intimidating task for radiologists due to their enormously overlaying sonographic presences. So, it is expected that the extraction of discriminatory features which are difficult to extract visually, followed by an efficient classifier design with a comprehensive data set consisting of representative images for various sub classes can reduce this limitation.

In the present work, the main focus is on the aspect of variations in texture patterns shown by focal kidney lesions. In order to visualise these textural disparities, texture features are calculated using different methods namely statistical features and spectral texture features. These texture features have been calculated from areas of interest (AOIs) extracted from each image within the lesion. For the classification task, kernel based SVM classifier has been used.

5.2 Proposed CAD System Design

The CAD system for the characterization of AML and RCC lesions has been proposed in the present study. The main purpose of emerging such a CAD system is to support radiologists, by providing additional diagnostic information to discriminate between AMLs and RCCs anomalies which might be sometimes missed by radiologists on visual observation. Thus, distinction between small RCCs and AMLs is crucial. Therefore in

this work, a CAD system design has been anticipated for differentiating the primary benign kidney lesions from primary malignant kidney lesions.

The block diagram of the proposed CAD system design for two-class classification of kidney using statistical and spectral texture features is shown in Figure 5.1.

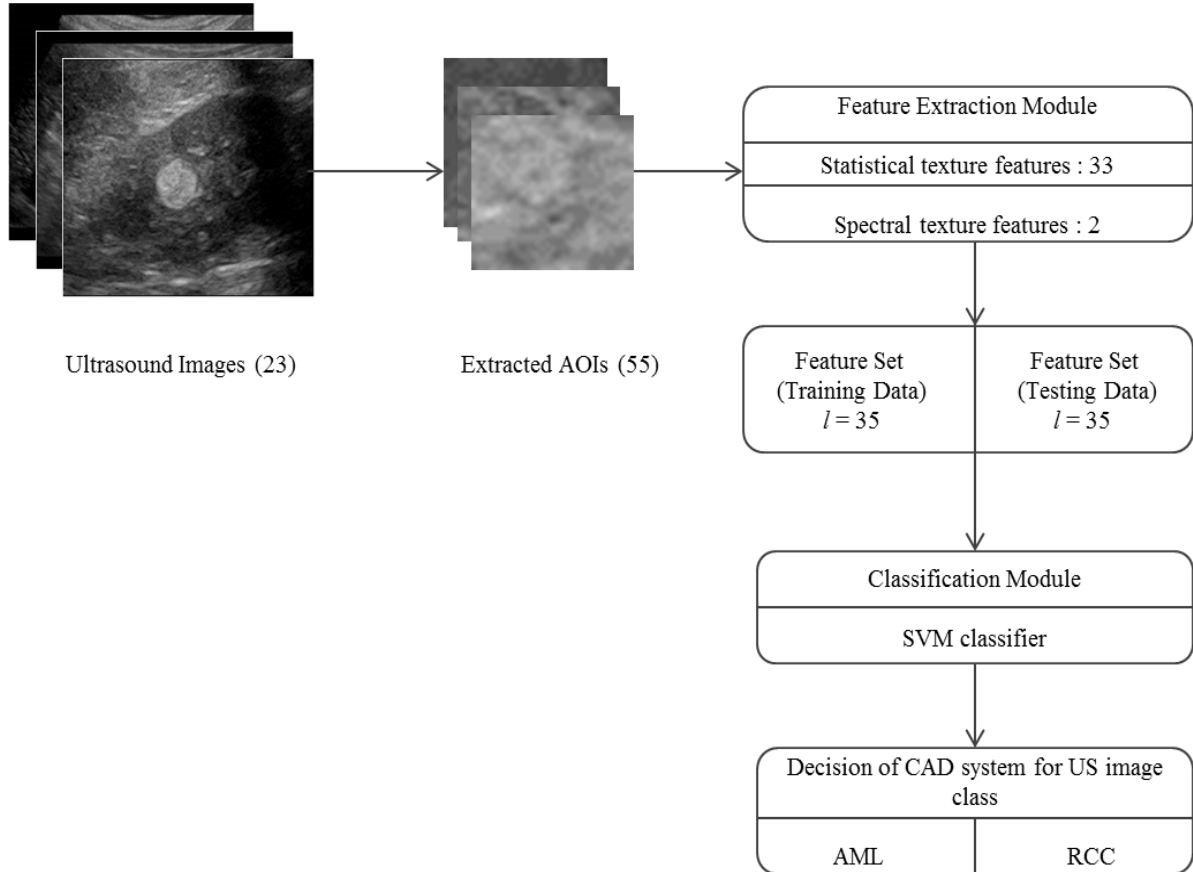


Figure 5.1: Block diagram representation of proposed Computer aided diagnosis system design for two class classification. Note: l : Length of feature set.

The CAD system is comprised of AOI extraction module, feature extraction module and classification module. The description of these modules is shown in below sections.

5.2.1 Dataset Description Module

In this work, a publically available benchmark database of 23 ultrasound kidney images has been used. The images in the database are classified into two types namely, AML and RCC. Out of 23 B-mode kidney US images, 14 images are AML images and 9 images are RCC images. Size of each image is 300×225 pixels having 96 dpi vertical and horizontal resolutions with a gray scale comprising of 256 tones. The database of 23

images contains the nature and position of irregularity existing in the kidney. The digital images are attained from Aloka ultrasound scanning system and Hitachi high end ultrasound systems.

5.2.2 AOI Extraction Module

For calculating various texture features, the selection of Area of Interest (AOI) size should be chosen carefully in such a way so that it should deliver adequate number of pixels. In earlier studies, it has been specified by many researchers that estimate reliable statistics size of AOI must be at least 800 pixels. For executing the CAD system design, out of 23 images of database 55 ROIs are manually extracted from inside the kidney lesion.

In AOI extraction module, from each lesion maximum non-overlapping AOIs of fixed size 32×32 are extracted manually. The participating radiologist recommended that, AOIs should be taken from within the lesions of kidney avoiding the renal sinus region which is a cavity consisting of fats, blood vessels, nerves, etc.

Images from the database with marked AOIs are illustrated in Figure 5.2.

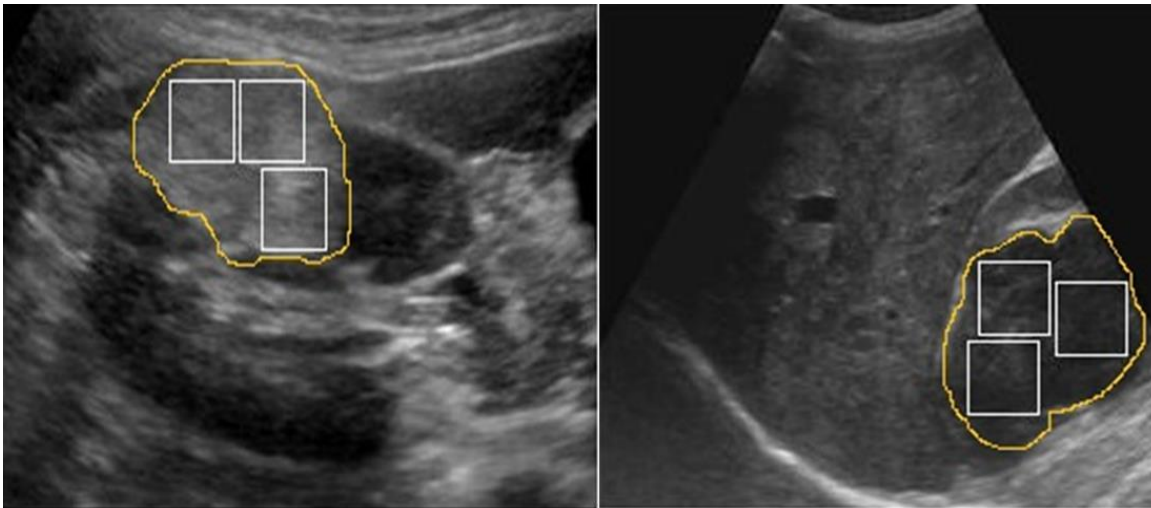


Figure 5.2: Images with marked AOIs. (a) AML image (b) RCC image

The distribution of the acquired database with 23 B-mode kidney US images among AML and RCC image classes and the division of AOIs in training and testing data set is shown in Figure 5.3.

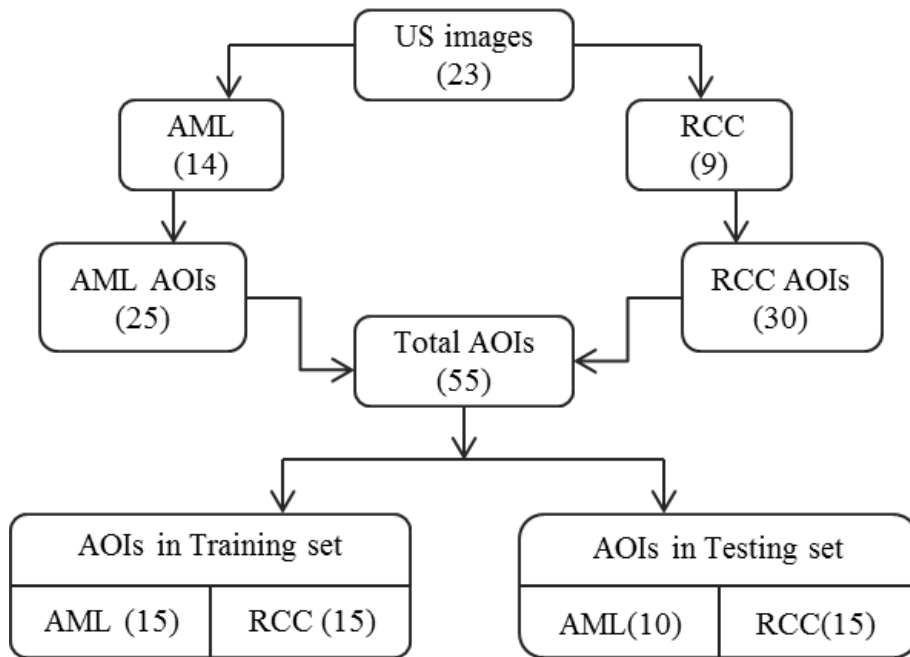


Figure 5.3: Description of dataset for two class classification.

5.2.3 Feature Extraction Module

In present work, feature extraction module is used to calculate the mathematical descriptors for understanding the fundamental AOI textural properties. These descriptors are either texture based features or shape based features (morphological features). The radiologist tells that, for the differential analysis between focal kidney lesions, only texture features gives the appropriate information. In the present work, various kind of textural features are calculated from AOI using numerous statistical texture features such as First order statistics (FOS), Higher order statistics , NGTDM features, SFM features, Edge features and spectral features such as Fourier power spectrum (FPS) features. In this study, 33 statistical features and 2 spectral texture features has been extracted.

The different types of feature extraction methods are illustrated in Figure 5.4 and the explanation of all these features has been already shown in chapter 3 in section 3.2.3.1 and section 3.2.3.2.

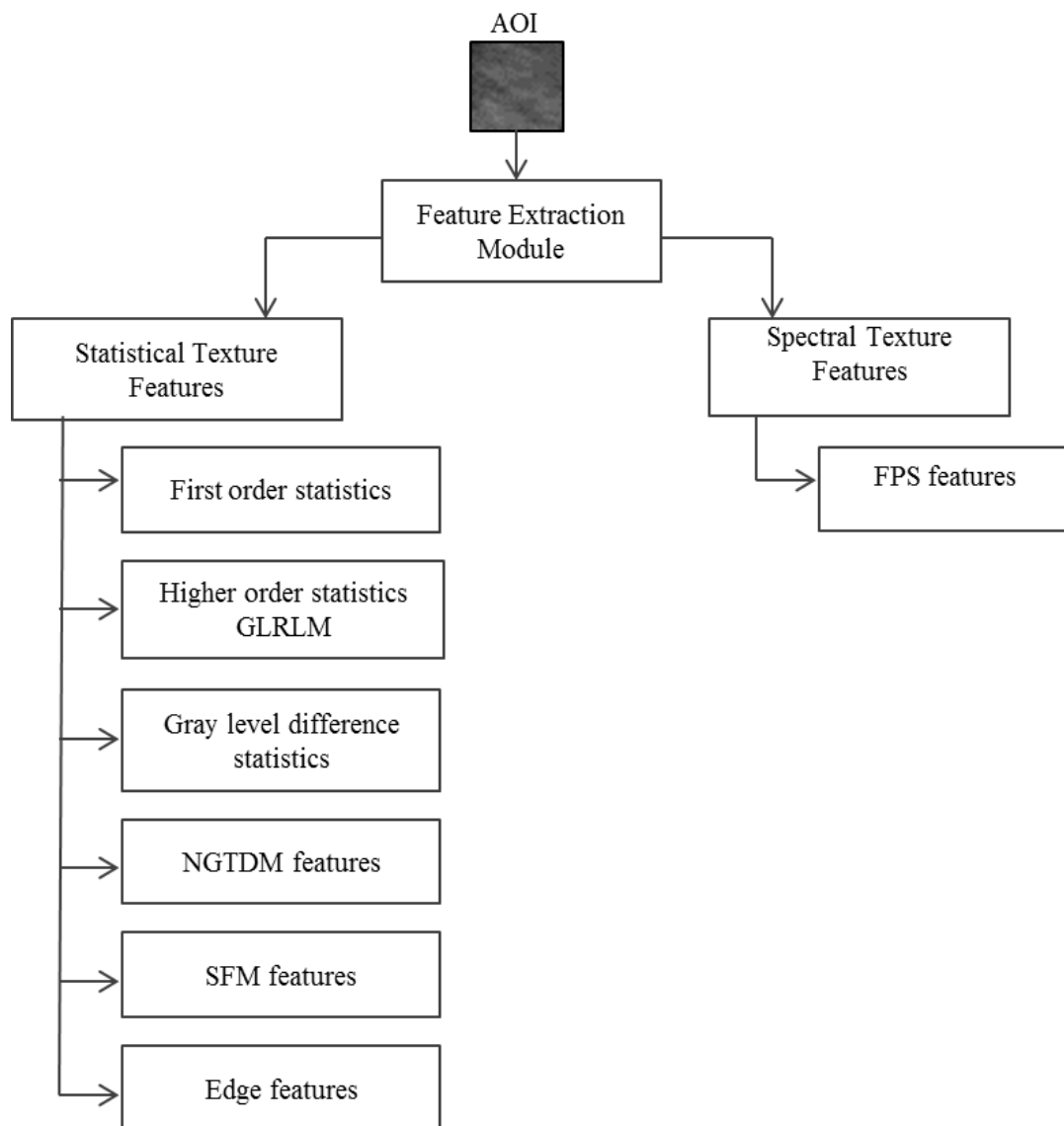


Figure 5.4: Texture features computed for each AOI image.

Note: GLRLM: Gray level run length matrix, NGTDM: Neighborhood gray tone difference matrix, SFM: Statistical feature matrix, FPS: Fourier power spectrum

From the above feature extraction methods, in Table 5.1 the following texture feature vectors (TFVs) have been computed.

Table 5.1: Description of extracted TFVs for the characterization of AML and RCC lesions

Features	TFV	Texture Features	l
Statistical features	TFV1	FOS features	6
	TFV2	GLRLM features	11
	TFV3	GLDS features	5
	TFV4	NGTDM features	5
	TFV5	SFM features	4
Spectral features	TFV6	Edge features	2
	TFV7	FPS features	2

Note: TFV: Texture feature vector, l : Length of TFV

5.3 Results and Discussion

For evaluating the performance of the proposed CAD system design, numerous experiments have been carried out in the present work to characterize the focal kidney lesions for two-class classification. A brief description of the conducted experiments for the primary kidney lesions classification is tabularized in Table 5.2

Table 5.2: Description of experiments carried out for two-class breast tissue density classification.

Experiment 1: To find the classification performance of statistical texture features for two-class kidney classification using SVM classifier.
Experiment 2: To find the classification performance of spectral texture features for two-class kidney classification using SVM classifier.
Experiment 3: To find the classification performance of combined texture features for two-class kidney classification using SVM classifier.

5.3.1 Experiment 1: To find the classification performance of statistical features for primary benign (AML) and primary malignant (RCC) Kidney lesions using SVM classifier.

In this experiment, different statistical features classification performance is measured using SVM classifier. The results of experiment 1 are depicted in Table 5.3.

Table 5.3: Result of Classification performance of statistical features using SVM classifier for two-classes of Kidney.

Features	CM			OCA (%)	ICA _{AML} (%)	ICA _{RCC} (%)
		AML	RCC			
FOS	AML	5	5	64.0	50.0	73.3
	RCC	4	11			
GLRLM	AML	6	4	76.0	60.0	86.6
	RCC	2	13			
GLDS	AML	3	7	24.0	30.0	20.0
	RCC	12	3			
NGTDM	AML	4	6	52.0	40.0	60.0
	RCC	6	9			
SFM	AML	4	6	36.0	40.0	33.3
	RCC	10	5			
Edge	AML	5	5	72.0	50.0	86.6
	RCC	2	13			

Note: CM: Confusion matrix, AML: Angiomyolipoma class, RCC: Renal Cell Carcinoma class, OCA: Overall classification accuracy, ICA_{AML}: Individual class accuracy for angiomyolipoma, ICA_{RCC}: Individual class accuracy for renal cell carcinoma.

From the table 5.3 it has been observed that, from GLRLM features, the highest overall classification accuracy (OCA) of 76.0 % is achieved for this statistical features using SVM classifier. It is also observed in this experiment that the maximum individual class accuracy (ICA) for AML class is 60.0 % and maximum individual class accuracy for RCC class is 86.6 %. Out of 25 testing cases, 19 cases (19/25) are correctly classified and 6 cases (6/25) are not correctly classified in GLRLM feature.

5.3.2 Experiment 2: To find the classification performance of spectral features (Fourier Power Spectrum (FPS) texture features) for primary benign (AML) and primary malignant (RCC) Kidney lesions using SVM classifier.

In this experiment, FPS features classification performance is assessed using SVM classifier. The results of experiment 2 are depicted in Table 5.4.

Table 5.4: Result of Classification performance of Fourier Power Spectrum features using SVM classifier for two-classes of kidney

Features	CM		OCA (%)	ICA _{AML} (%)	ICA _{RCC} (%)
	AML	RCC			
FPS	AML	8	72.0	80.0	66.6
	RCC	10			

Note: CM: Confusion matrix, AML: Angiomyolipoma class, RCC: Renal Cell Carcinoma class, OCA: Overall classification accuracy, ICA_{AML}: Individual class accuracy for angiomyolipoma, ICA_{RCC}: Individual class accuracy for renal cell carcinoma

From the table 5.4 it has been observed that, for Fourier Power Spectrum texture features, the maximum classification accuracy of 72.0 % is achieved using SVM classifier. It is also observed from this experiment that the maximum individual class accuracy for AML is 80.0 % and maximum individual class accuracy for RCC is 66.6 %. Out of 25 testing cases, 18 cases (18/25) are correctly classified and 7 cases (7/25) are not correctly classified in FPS feature by using SVM classifier.

From experiment 1 and experiment 2, it can be observed that amongst statistical texture features, higher order statistics based GLRLM features (TFV2) yield the highest classification accuracy of 76% and the second highest classification accuracy of 72% is achieved with spectral domain FPS features (TFV7).

5.3.3 Experiment 3: To find the classification performance of combined texture features ((GLRLM + FPS) features) for primary benign (AML) and primary malignant (RCC) Kidney lesions using SVM classifier.

Another experiment, experiment no. 3 has been conducted to evaluate the performance of combined feature vector (CFV) consisting of higher order GLRLM features and FPS features (CFV = TFV2 + TFV7). In this experiment, combined features (statistical and spectral features) classification performance is measured using SVM classifier. The results of experiment 3 are depicted in Table 5.5.

Table 5.5: Result of Classification performance of combination of statistical and spectral features using SVM classifier for two-classes of kidney.

Features	CM		OCA (%)	ICA _{AML} (%)	ICA _{RCC} (%)
	AML	RCC			
GLRLM + FPS			84.0	60.0	100.0
	AML	6			
	RCC	0			

Note: CM: Confusion matrix, AML: Angiomyolipoma class, RCC: Renal Cell Carcinoma class, OCA: Overall classification accuracy, ICA_{AML}: Individual class accuracy for angiomyolipoma, ICA_{RCC}: Individual class accuracy for renal cell carcinoma

From the table 5.5 it has been observed that, by CFV comprising of GLRLM and FPS features, the maximum overall classification accuracy of 84.0 % is achieved with individual class accuracy of 100 % for RCC and with individual class accuracy of 60% for AML. Out of 25 testing cases, 21 cases (21/25) are correctly classified and 4 cases (4/25) are not correctly classified by using SVM classifier.

5.4. Concluding Remarks

This work indicates that a study on the characterization of focal kidney lesions has been carried out. From the rigorous experimentation it can be observed that, for the classification of focal kidney lesions, the CAD system gives the highest OCA of 84.0 % from SVM classifier. It can be concluded that, for the differential analysis between primary benign and primary malignant kidney lesions, the performance of CFV i.e. combined feature vectors are obtained by combining TFV2 (Gray level run length matrix (GLRLM) feature) with TFV7(Fourier Power Spectrum (FPS) feature) provide the highest OCA of 84.0 %. CFV also give the highest individual class accuracy (ICA) of 100 % for RCC. Therefore, combination of these two features (GLRLM+FPS) is important for achieving best results which accounts for the textural variations shown by the primary focal lesions.

The attained results of proposed CAD system design specify their effectiveness to support radiologists for the differential diagnosis of AML and RCC kidney lesions during regular medical check-ups.

CHAPTER 6

CAD SYSTEM DESIGN FOR CLASSIFICATION OF FOCAL KIDNEY LESIONS USING WAVELET BASED TEXTURE DESCRIPTORS

6.1 Introduction

The differential discrimination of primary focal kidney lesions such as angiomyolipomas and renal cell carcinomas is a daunting challenge for radiologists due to their immensely overlapping sonographic presences. Therefore a decision making CAD system for the classification of the different focal kidney lesions from US images is highly required.

Thus, a CAD system design is proposed in this chapter for the classification of focal kidney lesions using various wavelet energy descriptors and a support vector machine (SVM) classifier has been used for the classification task. The focal kidney lesions are categorized into two kidney classes namely primary benign i.e. angiomyolipoma (AML) and primary malignant i.e. renal cell carcinoma (RCC). The multi-resolution wavelet based texture descriptors are calculated from area of interests (AOIs) of variable sizes by using different types of wavelet filters such as Haar, Daubechies, biorthogonal, symlets and coiflets filters.

6.2 Proposed CAD System Design

For enhancing the confidence level of radiologists, the CAD systems are used in the medical imaging as a second opinion tool. The objective of emerging a decision making CAD system is, to support radiologists and other health professionals by providing extra diagnostic information in image reading and to differentiate between various anomalies. In the present study, it has been described that when size of AMLs are less than 2cms, radiologists get confused with small size RCCs and thus the chances of uncertainty increases for the discrimination between small RCCs and small AMLs. Therefore, CAD

system has been proposed for differential diagnosis between focal kidney lesions by using kidney US images. The CAD system mainly consists of three blocks namely AOI extraction module, feature extraction module and classification module. The description of these modules is shown in below sections.

Figure 6.1 shows the block diagram of the proposed CAD system design for the prediction of kidney lesions.

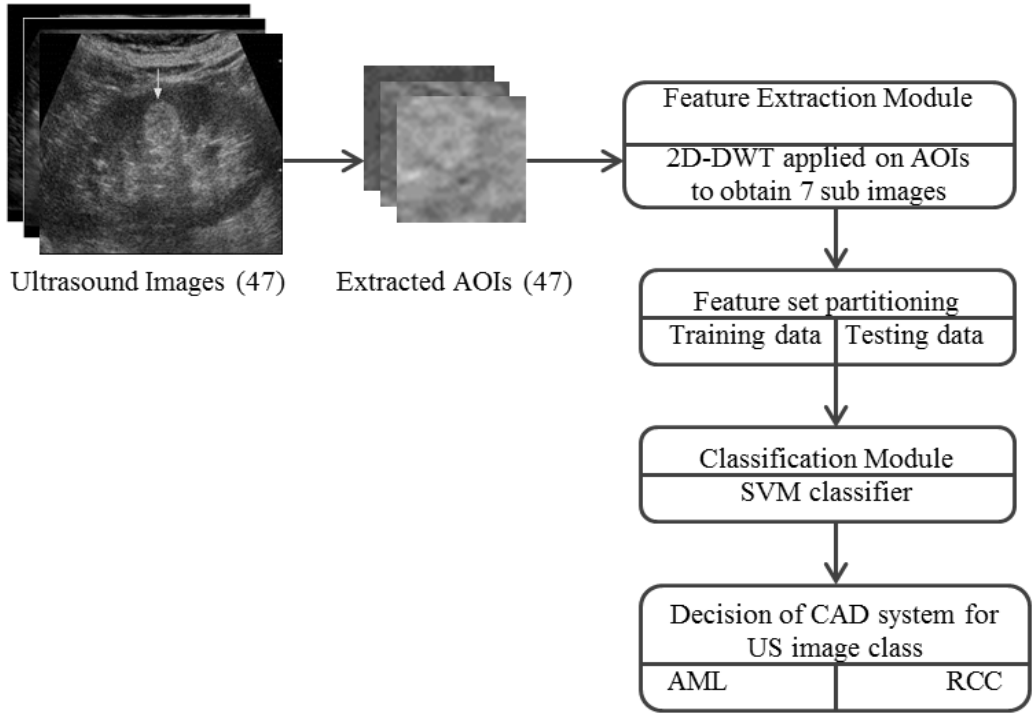


Figure 6.1: Block diagram representation of proposed CAD system design

6.2.1 Dataset Description Module

In this work, a publically available benchmark database has been used. The images in the database are classified into two types namely, AML and RCC. The database contains 47 B- mode kidney US images (22 images of AML lesion and 25 images of malignant lesion). Each image is of the size of 300 × 225 pixels having 96 dpi horizontal and vertical resolutions with 256 gray scale tones. The digital images are obtained from Aloka ultrasound scanning system and Hitachi high end ultrasound systems.

6.2.2 AOI Extraction Module

The size of Area of Interest (AOI) has been selected wisely in such a manner that it must deliver a good statistical population for making the correct decisions in CAD system. For the CAD system execution, total 47 images of database has been taken, out of which total 47 single AOIs are extracted manually. In AOI extraction module, from each ultrasonographic image, single AOI of variable sizes are extracted manually from within the lesions of kidney. Depending on the size of lesions, the largest rectangular AOI has been cropped from the region inside the lesion. The participating radiologist opined that the shape or margin features are not important for differential diagnosis between focal kidney lesions. Therefore an attempt has been made to take the largest AOI from each lesion leaving the boundary of the lesion so as to compute reliable estimates of texture features.

In the present work, single AOI of variable sizes such as 32×32 , 40×40 , 64×64 , 96×96 , 100×100 , 128×128 etc. are manually extracted from within the lesion. The data set contains total 47 AOIs with 22 AML AOIs (from 22 AML kidney images) and 25 RCC AOIs (from 25 RCC images)

Sample images with extracted AOIs from focal kidney lesions are shown in Figure 6.2.

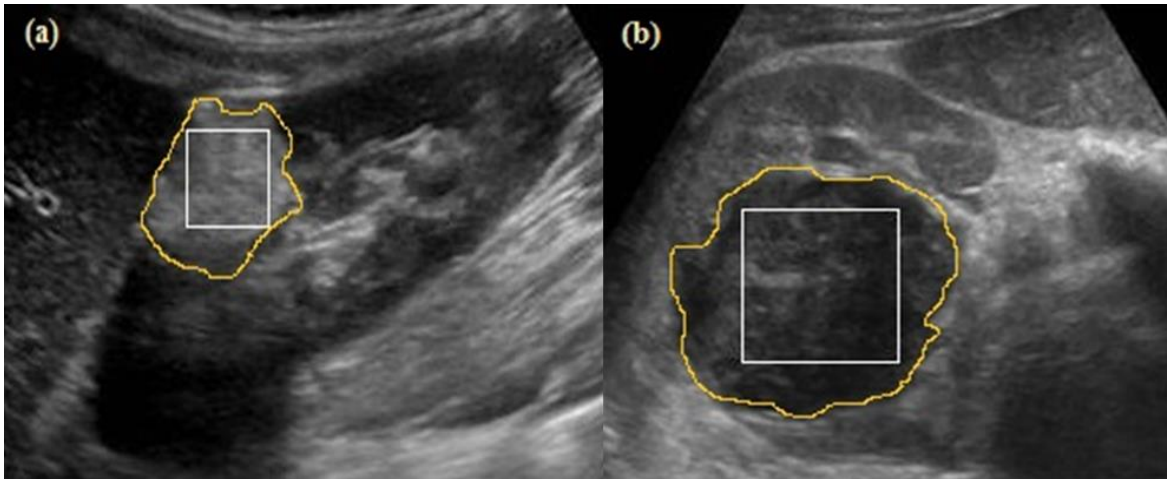


Figure 6.2: Images of extracted AOIs. (a) AML image (b) RCC image

6.2.3 Feature Extraction Module

In this study, various kinds of texture features are calculated from AOIs using numerous wavelet energy descriptors. The dataset is distributed into training and testing dataset. By using multi-resolution scheme such as discrete wavelet transform (DWT), feature

extraction is carried out in transform domain over various scales. In various studies, it has been shown that the effective depiction of texture depends upon the wavelet filter properties. Therefore in order to obtain the best wavelet filter for the present task of kidney lesions classification, ten dissimilar compact support wavelet filters (basis wavelet functions) such as Biorthogonal (bior3.1, bior3.3 and bior4.4), Coiflets (coif1 and coif2), Haar (db1), Daubechies (db4 and db6) and Symlets (sym3 and sym5) filters have been used to obtain sub-band images for each AOI image. Each compact support wavelet filter consists of seven texture feature vectors. By using 2D-DWT (Discrete wavelet transform), when AOI image is decomposed up to 2nd level, then one approximate sub image and six orientation detail sub images are generated. From the obtained sub images, normalized energy is calculated. Total seven wavelet energy descriptors chosen as texture feature vectors (TFVs) are shown in Table 6.1. TFV1 consists of 7 features, TFV2 consists of 3 features, TFV3 consists of 6 features, TFV4 consists of 4 features, TFV5 consists of 4 features, TFV6 consists of 4 features and TFV7 consists of 3 features are shown in Table 6.1.

Table 6.1: Description of Seven wavelet energy descriptors as TFVs.

TFV	Wavelet energy descriptors in TFVs	<i>l</i>
TFV1	$\left(\frac{\ A_2\ _F^2}{\text{area}(A_2)}, \frac{\ D_2^{(h)}\ _F^2}{\text{area}(D_2^{(h)})}, \frac{\ D_2^{(v)}\ _F^2}{\text{area}(D_2^{(v)})}, \frac{\ D_2^{(d)}\ _F^2}{\text{area}(D_2^{(d)})}, \frac{\ D_1^{(h)}\ _F^2}{\text{area}(D_1^{(h)})}, \frac{\ D_1^{(v)}\ _F^2}{\text{area}(D_1^{(v)})}, \frac{\ D_1^{(d)}\ _F^2}{\text{area}(D_1^{(d)})} \right)$	7
TFV2	$\left(\frac{\ D_1^{(h)}\ _F^2}{\text{area}(D_1^{(h)})}, \frac{\ D_1^{(v)}\ _F^2}{\text{area}(D_1^{(v)})}, \frac{\ D_1^{(d)}\ _F^2}{\text{area}(D_1^{(d)})} \right)$	3
TFV3	$\left(\frac{\ D_2^{(h)}\ _F^2}{\text{area}(D_2^{(h)})}, \frac{\ D_2^{(v)}\ _F^2}{\text{area}(D_2^{(v)})}, \frac{\ D_2^{(d)}\ _F^2}{\text{area}(D_2^{(d)})}, \frac{\ D_1^{(h)}\ _F^2}{\text{area}(D_1^{(h)})}, \frac{\ D_1^{(v)}\ _F^2}{\text{area}(D_1^{(v)})}, \frac{\ D_1^{(d)}\ _F^2}{\text{area}(D_1^{(d)})} \right)$	6
TFV4	$\left(\frac{\ D_1^{(h)}\ _F^2}{\text{area}(D_1^{(h)})}, \frac{\ D_1^{(v)}\ _F^2}{\text{area}(D_1^{(v)})}, \frac{\ D_1^{(d)}\ _F^2}{\text{area}(D_1^{(d)})}, \frac{\ D_2^{(d)}\ _F^2}{\text{area}(D_2^{(d)})} \right)$	4
TFV5	$\left(\frac{\ A_2\ _F^2}{\text{area}(A_2)}, \frac{\ D_1^{(h)}\ _F^2}{\text{area}(D_1^{(h)})}, \frac{\ D_1^{(v)}\ _F^2}{\text{area}(D_1^{(v)})}, \frac{\ D_1^{(d)}\ _F^2}{\text{area}(D_1^{(d)})} \right)$	4
TFV6	$\left(\frac{\ A_2\ _F^2}{\text{area}(A_2)}, \frac{\ D_2^{(h)}\ _F^2}{\text{area}(D_2^{(h)})}, \frac{\ D_2^{(v)}\ _F^2}{\text{area}(D_2^{(v)})}, \frac{\ D_2^{(d)}\ _F^2}{\text{area}(D_2^{(d)})} \right)$	4
TFV7	$\left(\frac{\ D_2^{(h)}\ _F^2}{\text{area}(D_2^{(h)})}, \frac{\ D_2^{(v)}\ _F^2}{\text{area}(D_2^{(v)})}, \frac{\ D_2^{(d)}\ _F^2}{\text{area}(D_2^{(d)})} \right)$	3

Note: TFV: Texture feature vector, *l*: length of TFV, A: Approximate sub image, D: Detail sub image, h: horizontal direction, v: Vertical direction, d: Diagonal direction, F: Frobenius norm. A_i or D_i is the level of decomposition

The description of basis wavelet functions such as Haar, Daubechies, Symlets, Coiflets and Biorthogonal are shown in sections 6.2.3.1, 6.2.3.2, 6.2.3.3, 6.2.3.4 and 6.2.3.5.

6.2.3.1 Haar Wavelets (db1)

Haar wavelet is one of the simplest feasible wavelet functions and is supported by orthogonal wavelets. The basis vectors of the Haar matrix are serially ordered. The Haar wavelet is not continuous and it looks like a step function. This wavelet function is a sequence of rescaled square-shaped functions which collectively form a wavelet family.

6.2.3.2 Daubechies Wavelets (db)

Daubechies wavelet is based on the work of Ingrid Daubechies. They are a family of orthogonal wavelets which defines a discrete wavelet transform (DWT). Daubechies wavelet transform signal is well-defined by the wavelet and scaling functions that are articulated in terms of β coefficients.

6.2.3.3 Symlets Wavelets

Symlets are virtually symmetrical wavelets which define a family of orthogonal wavelets and are proposed by Daubechies as alterations to the db family. This wavelet is also named as "least asymmetric" wavelet.

6.2.3.4 Coiflets Wavelets

Coiflets wavelets are similar to Daubechies wavelets upto certain level, but the Coiflet is erected with vanishing moments for wavelet function $\varphi(x)$ as well as for scaling function $\phi(x)$.

6.2.3.5 Biorthogonal Wavelets

A biorthogonal wavelet is a wavelet function where the related wavelet transform is not essentially orthogonal, but is invertible. Biorthogonal wavelets have more degrees of freedom than orthogonal wavelets. Biorthogonal wavelets encompass the family of orthogonal wavelets and have the property of linear phase

6.3 Results and Discussion

For evaluating the performance of the proposed CAD system design, severe experimentation has been done in this work to obtain the classification performance and to discriminate primary kidney lesions using various wavelet energy descriptors with SVM classifier.

6.3.1 To obtain the classification performance of seven wavelet energy descriptors (TFV1-TFV7) derived from various compact support wavelet filters for two-classes (AML and RCC) of kidney using SVM classifier.

In this experiment, SVM classifier is used to get the classification performance of wavelet energy features. The results of experiment are depicted in Table 6.2 and Table 6.3.

Table 6.2: Classification performance of TFVs using SVM classifier.

TFV	<i>l</i>	Max. Acc. (%)	Wavelet filter	Min. Acc. (%)	Wavelet filter
TFV1	7	82.6	db4	60.8	bior3.1, bior3.3
TFV2	3	52.1	bior3.3	39.1	db4
TFV3	6	82.6	sym3	52.1	bior3.1, db1
TFV4	4	78.2	coif2, db4	43.4	bior3.3
TFV5	4	78.2	bior3.1	47.8	db4, coif2
TFV6	4	69.5	bior3.3	56.5	bior4.4, coif1, sym3
TFV7	3	65.2	bior3.1	52.1	coif1, coif2, db4, db6, sym5

Note: *l*: Length of TFV, Max. Acc.: Maximum accuracy, Min. Acc.: Minimum accuracy

From table 6.2, it is observed that out of all seven TFVs, the maximum accuracy is attained from db4 (Daubechies) and sym3 (Symlets) wavelet filters. It is also seen that highest overall classification accuracy (OCA) of 82.6 % is achieved for db4 and sym 3 filters with TFV1 and TFV3 using SVM classifier. The minimum classification accuracy of 39.1 % is achieved for db4 wavelet filter using SVM classifier. The result of best TFVs is shown below in Table 6.3.

Table 6.3: Classification performance of the best TFVs using SVM classifier.

TFV	CM		OCA (%)	ICA _{AML} (%)	ICA _{RCC} (%)	
TFV1		AML	RCC	82.6	63.6	100.0
	AML	7	4			
TFV3	RCC	0	12	82.6	63.6	100.0
	AML	7	4			
	RCC	0	12			

Note: CM: Confusion matrix, AML: Angiomyolipoma class, RCC: Renal Cell Carcinoma class, OCA: Overall classification accuracy, ICA_{AML}: Individual class accuracy for angiomyolipoma, ICA_{RCC}: Individual class accuracy for renal cell carcinoma

From table 6.3, it is observed that TFV1 and TFV3 give the maximum accuracy of 82.6 %. It is also observed from this experiment that the maximum individual class accuracy for AML is 63.6 % and maximum individual class accuracy for RCC is 100 %. Out of 23 testing cases, 18 cases (19/23) are correctly classified and 4 cases (4/23) are misclassified by using SVM classifier.

6.4. Concluding Remarks

In the present work, a CAD system for the classification of primary focal kidney lesions has been developed by multi-resolution texture analysis of kidney US images. From the above experimentation it can be concluded that, for the characterization of focal kidney lesions, wavelet energy descriptors i.e. db4 and sym3 filters contain significant information. These wavelet filters provides the highest OCA of 82.6 % and gives the highest individual class accuracy (ICA) of 100 % for RCC.

Therefore, SVM based CAD system design employing wavelet based texture features is the best choice for discerning between primary benign and primary malignant focal kidney lesions.

Thus, the obtained results of a decision making system design state their helpfulness to support radiologists to distinguish between AML and RCC kidney lesions during routine medical check-ups.

CHAPTER 7

CONCLUSION AND FUTURE SCOPE

7.1 Conclusion

The key objective of the research work existing in the thesis is to improve the analytic prospective of conventional gray scale B-Mode ultrasound for the diagnosis of kidney diseases by emerging effective computerized tissue characterization (CAD) system designs using a comprehensive and representative image database. A study in this thesis has been carried out on the classification of kidney lesions. The CAD system design for the classification of primary benign and primary malignant kidney lesions using Statistical and Spectral Texture Features has been evaluated.

Accordingly, different CAD system designs have been proposed in the present work for two-class kidney classification to provide radiologists with a second opinion device.

7.2 Conclusion- Design of an Efficient CAD System for Classification of Focal Kidney Lesions Using Texture Features

For the design of an efficient CAD system for two-class kidney classification, extensive experimentation was carried out in the present work by using statistical features, spectral features and multiresolution texture features. The performance of the proposed CAD system designs based on these features is compared in Table 7.1

Table 7.1: Performance comparison of CAD system designs for two-class kidney classification using SVM classifier.

Features	CAD design	OCA (%)
GWT	CAD System Design for Classification of Focal Kidney Lesions Using Gabor Wavelet Texture Features	90.0

GLRLM+FPS	CAD System Design for Characterization of Focal Kidney Lesions Using Statistical and Spectral Texture Features	84.0
TFV1 (db4) TFV3 (sym3)	CAD System Design for Classification of Focal Kidney Lesions Using Wavelet Based Texture Descriptors	82.6

Note: GWT: Gabor wavelet transform, GLRLM: Gray level run length matrix, FPS: Fourier power spectrum, TFV: Texture feature vector, OCA: Overall classification accuracy.

From the Table 7.1, it can be observed that by using SVM classifier, CAD system design based on Gabor wavelet texture features achieves maximum classification accuracy of 90.0 % out of all the proposed CAD system designs for the classification of focal kidney lesions. It can be concluded that the Gabor wavelet texture features are thus most useful and efficient texture features to account for the textural variations of focal kidney lesions when fed to SVM classifier for predicting the labels unknown testing instances of the US images.

From the above discussion it can be concluded that Gabor wavelet transform features efficiently classify the small AML and small RCC lesions and achieves best result in comparison to CAD system designs based on other feature extraction models.

7.3 Limitations and Future Scope

The limitation of the present work is that it has been carried out on the publically available benchmark database that consists of digitized ultrasound images and not real data.

Following are the recommendations for future work:

(i) The present work has been carried out on benchmark database images for analysis of kidney focal lesions. In future, we can use a real time database to evaluate the performance of the proposed CAD system.

(ii) The present work has been carried out on images developed using ultrasound as the imaging modality however, images acquired from MRI can also be used in the future to test the proposed algorithm.

(iii) In the present work, AOIs from the ultrasound images are extracted manually.

Automatic AOI extraction algorithm can be developed by employing various pattern recognition concepts to identify the lesions of the kidney and then extract an AOI of some specified size automatically.

(iv) This work can be further extended by extracting the ratio features from inside the lesions and from the parenchyma region.

(v) The presentation of the proposed procedures remains to be tested on images of different resolutions as the images used in the present work has been attained from the single ultrasound machine.

Publications from the Present Work

Referred Journal Publications

- 1) S. Rana, S. Jain, and J. Virmani, "SVM-Based Characterization of Focal Kidney Lesions from B-Mode Ultrasound Images", *Research Journal of Pharmaceutical, Biological and Chemical Services*, vol. 7, no. 4, 2016. [Accepted]
- 2) S. Rana and S. Jain, "Classification of Focal Kidney lesions using Wavelet-Based Texture Descriptors", *International Journal of Pharma and Bio Sciences*, vol. 7, no. 3, 2016. [Accepted]

Referred Conference Publications

- 1) S. Rana, S. Jain, and J. Virmani, "Classification of Kidney Lesions using Gabor Wavelet Texture Features", *In Proceedings of the 10th INDIACom 3rd 2016 International Conference on Computing for Sustainable Global Development*, New Delhi, 16th –18th March, 2016, pp. 2528-2532. [Accepted]

References

- [1] <http://www.veterinaryradiology.net/>.
- [2] O. Inci, M. Kalpan, O. Yalcin, I. H. Atakan, and H. Kubat, “Renal angiomyolipoma with malignant transformation, simultaneous occurrence with malignity and other complex clinical situations”, *International Urology and Nephrology*, vol. 38, pp. 417–426, 2006.
- [3] B. K. Raja, M. Madheswaran, and K. Thyagarajah, “A hybrid fuzzy-neural system for computer-aided diagnosis of ultrasound kidney images using prominent features”, *Journal of Medical Systems*, vol. 32, no. 1, pp. 65–83, 2008.
- [4] B. K. Raja, M. Madheswaran, and K. Thyagarajah, “Texture pattern analysis of kidney tissues for disorder identification and classification using dominant Gabor wavelet”, *Machine Vision and Applications*, vol. 21, no. 3, pp. 287–300, 2010.
- [5] B. K. Raja, M. Madheswaran, and K. Thyagarajah, “Ultrasound kidney image analysis for computerized disorder identification and classification using content descriptive power spectral features”, *Journal of Medical Systems*, vol. 31, no. 5, pp. 307–317, 2007.
- [6] J. Susan Jose, R. Sivakami, N. Uma Maheswari, and R. Venkatesh, “An Efficient Diagnosis of Kidney Images Using Association Rules”, *International Journal of Computer Technology and Electronics Engineering (IJCTEE)*, vol. 2, no. 2, 2012.
- [7] T. P. Akkasaligar and S. Biradar, “Classification of Medical Ultrasound Images of Kidney”, *International Conference on Information and Communication Technologies (ICICT)*, 2014.
- [8] M. B. Subramanya, Vinod Kumar, Shaktidev Mukherjee, and Manju Saini, “SVM-Based CAC System for B-Mode Kidney Ultrasound Images”, *Journal of Digital Imaging*, DOI 10.1007/s10278-014-9754-4, Society for Imaging Informatics in Medicine, 2014.
- [9] B. K. Raja, M. Madheswaran, and K. Thyagarajah, “Analysis of ultrasound kidney images using content descriptive multiple features for disorder identification and ANN based classification”, *International conference on Computing, Theory and Applications, ICCTA'07*, 2007, pp. 382–388.
- [10] B. K. Raja, M. Madheswaran, and K. Thyagarajah, “Evaluation of tissue characteristics of kidney for diagnosis and classification using first order statistics and RTS

invariants”, *In Proceedings of IEEE International Conference on Signal Processing, Communications and Networking, ICSCN’07*, 2007, pp. 483–487.

[11] Ultrasound cases from the teaching files from the Gelderse Vallei Hospital in Ede, the Netherlands, <http://www.ultrasoundcases.info/>.

[12] J. Suckling, J. Parker, D. R. Dance, S. Astley, I. Hutt, C. R. M. Boggis, I. Ricketts, E. Stamatakis, N. Cerneaz, S. L. Kok, P. Taylor, D. Betal, and J. Savage, “The mammographic image analysis society digital mammogram database”, *In Digital Mammography*, E. G. Gale et al., Eds., Berlin, Heidelberg: Springer, 1994, vol.1069, pp. 375-378.

[13] J. Virmani, V. Kumar, N. Kalra, and N. Khandelwal, “SVM-based characterization of liver ultrasound images using wavelet packet texture descriptors”, *Journal of Digital Imaging*, vol. 26, no. 3, pp. 530-543, 2013.

[14] C. M. Wu and Y. C. Chen, “Multi-threshold dimension vector for texture analysis and its application to liver tissue classification”, *Pattern Recogn*, vol. 26, no. 1, pp. 137–144, 1993.

[15] Y. M. Kadah, A. A. Farag, J. M. Zurada, A.M. Badawi, and A. M. Youssef, “Classification algorithms for quantitative tissue characterization of diffuse liver disease from ultrasound images”, *IEEE Trans Med Imaging*, vol. 15, no. 4, pp. 466–478, 1996.

[16] D. Balasubramanian, P. Srinivasan, and R. Gurupatham, “Automatic classification of focal lesions in ultrasound liver images using principal component analysis and neural networks”, *In Proceedings of 29th IEEE EMBS Annual International Conference, IEEE*, Lyon, France, 2007, pp. 23–26.

[17] S. Poonguzhali and G.Ravindran, “Automatic classification of focal lesions in ultrasound liver images using combined texture features”, *Inf Tech J*, vol. 7, no. 1, pp. 205–209, 2008.

[18] J. Virmani, V. Kumar, N. Kalra, and N. Khandelwal, “A rapid approach for prediction of liver cirrhosis based on first order statistics”, *In Proceedings of IEEE International Conference on Multimedia, Signal Processing and Communication Technologies, IMPACT-2011*, pp. 212–215.

- [19] D. Mitrea, S. Nedevschi, M. Lupsor, M. Socaciu, and R. Badea, “Experimenting various classification techniques for improving the automatic diagnosis of the malignant liver tumors based on ultrasound images”, *In Proceedings of International Conference on Image and Signal Processing, CISP-2010*, IEEE, Yantai, China, 2010.
- [20] S. H. Kim, J. M. Lee, K. G. Kim, J. H. Kim, J. Y. Lee, J. K. Han, and B. I. Choi, “Computer-aided image analysis of focal hepatic lesions in ultrasonography: preliminary results”, *Abdom Imaging*, vol. 34, no. 2, pp. 183- 191, 2009.
- [21] M. Rachidi, A. Marchadier, C. Gadois, E. Lespessailles, C. Chappard, and C. L. Benhamou, “Laws’ mask descriptors applied to bone texture analysis: an innovative and discriminant tool in osteoporosis”, *Skeletal Radiol*, vol. 37, no. 1, pp. 541- 548, 2008.
- [22] J. Virmani, V. Kumar, N. Kalra, and N. Khandelwal, “Characterization of primary and secondary malignant liver lesions from B-mode ultrasound”, *Journal of Digit Imaging*, vol. 26, no. 6, pp. 1058–1070, 2013.
- [23] J. Virmani, V. Kumar, N. Kalra, and N. Khandelwal, “PCA-SVM based CAD system for focal liver lesions from B-mode ultrasound”, *Def Sci J*, vol. 63, no. 5, pp. 478–486, 2013.
- [24] H. Yoshida, D. D. Casalino, B. Keserci, A. Coskun, O. Ozturk, and A. Savranlar, “Wavelet packet based texture analysis for differentiation between benign and malignant liver tumors in ultrasound images”, *Phys Med Biol*, vol. 48, no. 1, pp. 3735–3753, 2003.
- [25] S. Sujana, S. Swarnamani, and S. Suresh, “Application of artificial neural networks for the classification of liver lesions by image texture parameters”, *Ultrasound Med Biol*, vol. 22, no. 9, pp. 1177-1181, 1996.
- [26] S. Poonguzhali, Deepalakshmi, and G. Ravindran, “Optimal feature selection and automatic classification of abnormal masses in ultrasound liver images”, *In Proceedings of IEEE International Conference on Signal Processing, Communications and Networking, ICSCN’07*, 2007, pp. 503-506.
- [27] J. Virmani, V. Kumar, N. Kalra, and N. Khandelwal, “A comparative study of computer-aided classification systems for focal hepatic lesions from B-mode ultrasound”, *Journal of Medical Engineering and Technology*, vol. 37, pp. 292-306, 2013.
- [28] R. Haralick, K. Shanmugam, and I. Dinstein, “Textural features for image classification”, *IEEE Trans Syst Man Cybern SMC*, vol. 3, no. 6, pp. 610-121, 1973.

- [29] J. Virmani, V. Kumar, N. Kalra, and N. Khandelwal, "Prediction of cirrhosis based on singular value decomposition of gray level co-occurrence matrix and a neural network classifier", *In Proceedings of Development in E-systems Engineering, DeSE*, Dubai, 2011, pp. 146-151.
- [30] D. H. Xu, A. S. Kurani, J. D. Furst, and D. S. Raicu, "Run-Length Encoding for Volumetric Texture", *Heart*, 2004, vol.2, pp. 25-30.
- [31] F. Albrechtsen, "Statistical texture measures computed from gray level run length matrices", *Image*, vol.1, pp. 3-8, 1995.
- [32] J. Virmani, V. Kumar, N. Kalra, and N. Khandelwal, "Prediction of cirrhosis from liver ultrasound B-mode images based on Laws' mask analysis", in *Proceedings of IEEE International Conference on Image Information Processing, ICIIIP-2011*, Himachal Pradesh, India, 2011, pp. 1-5.
- [33] R. M. Galloway, "Texture analysis using gray level run lengths", *Comput Graph Image Process*, vol. 4, no. 1, pp. 172-179, 1975.
- [34] A. Chu, C. M. Sehgal, and J. F. Greenleag, "Use of gray level distribution of run lengths for texture analysis", *Pattern Recogn Lett*, vol. 11, no. 1, pp. 415-420, 1990.
- [35] B. V. Dasarathy and E. B. Holder, "Image characterizations based on joint gray level-run length distributions", *Pattern Recogn Lett*, vol. 12, no. 1, pp. 497-502, 1991.
- [36] G. Castellano, L. Bonilha, L. M. Li, and F. Cendes, "Texture analysis of medical images", *Clinical Radiology*, vol.59, pp. 1061-1069, 2004.
- [37] C. Castella, K. Kinkel, M. P. Eckstein, P. E. Sottas, F. R. Verdun, and F. Bochud, "Semiautomatic Mammographic Parenchymal Patterns Classification Using Multiple Statistical Features", *Academic Radiology*, vol.14, no. 12, pp. 1486-1499, 2007.
- [38] M. Amadasun and R. King, "Textural features corresponding to textural properties", *IEEE Transactions on Systems, Man and Cybernetics*, vol. 19, pp.1264-1274, 1989.
- [39] J. S. Weszka, C. R. Dyer, and A. Rosenfeld, "A comparative study of texture measures for terrain classification", *IEEE Transactions on Systems, Man and Cybernetics*, vol. 6, pp. 269-285, 1976.
- [40] J. K. Kim, and H. W. Park, "Statistical Textural Features for Detection of Microcalcifications in Digitized Mammograms", *IEEE Transactions on Medical Imaging*, vol.18, no. 3, pp. 231-238, 1999.

- [41] K. I. Laws, "Rapid texture identification", in *Proceedings of SPIE Image Processing for Missile Guidance*, 1980, pp. 376-380.
- [42] J. Virmani, V. Kumar, N. Kalra, and N. Khandelwal, "Prediction of liver cirrhosis based on multiresolution texture descriptors from B-mode ultrasound", *International Journal of Convergence Computing*, vol. 1, pp. 19-37, 2013.
- [43] C. C. Lee and S. H. Chen, "Gabor wavelets and SVM classifier for liver diseases classification from CT images", In *Proceedings of IEEE International Conference on Systems, Man and Cybernetics*, Taipei, Taiwan, 2006, pp. 548-552.
- [44] X. Li and Z. Tian, "Wavelet energy signature: comparison and analysis", in *Neural Information Processing*, I. King, J. Wang, L.W. Chan and D.L. Wang, Eds., Heidelberg, Berlin: Springer, vol. 4233, pp. 474-480, 2006.
- [45] J. G. Daugman, "An information-theoretic view of analog representations in the striate cortex", In *Computational Neuroscience*, E.L. Schwartz, Ed. Cambridge: MIT Press, 1990, pp.403-424.
- [46] A. Yazdani, T. Ebrahimi, and U. Hoffmann, "Classification of EEG signals using Dempster-Shafer theory and a k -nearest neighbor classifier", In *Proceedings of 4th International IEEE EMBS Conference on Neural Engineering*, Antalya, Turkey, 2009, pp. 327-330.
- [47] Y. Wu, K. Ianakiev, and V. Govindaraju, "Improved kNN classification", *Pattern Recognition*, vol. 35, pp. 2311-2318, 2002.
- [48] M. L. Zhang and Z. H. Zhou, "A kNN based algorithm for multilabel classification", In *Proceedings of IEEE International Conference on Granular Computing*, Beijing, China, 2005, vol. 2, pp. 718-721.
- [49] D. F. Specht, "Probabilistic neural networks", *Neural Networks*, vol.1, pp. 109-118, 1990.
- [50] D. F. Specht and H. Romsdahl, "Experience with adaptive probabilistic neural network and adaptive general regression neural network", In *Proceedings of the IEEE International Conference on Neural Networks*, Orlando, Florida, 1994, vol. 2, pp. 1203-1208.
- [51] V. L. Georgiou, N. G. Pavlidis, K. E. Parsopoulos, and M. N. Vrahatis, "Optimizing the performance of probabilistic neural networks in a bioinformatics task", In *Proceedings of the EUNITE 2004 Conference*, 2004, pp. 34-40.

- [52] D. F. Specht, "Probabilistic Neural Networks for Classification, Mapping, or Associative Memory", *IEEE International Conference on Neural Networks*, July 1998, vol. 1, pp. 525-532.
- [53] C. C. Chang and C. J. Lin, "LIBSVM, a library of support vector machines", Software available at <http://www.csie.ntu.edu.tw/~cjlin/libsvm>, Accessed 15 Jan 2015.
- [54] C. J. C. Burges, "A tutorial on support vector machines for pattern recognition", *Data Min Knowl Disc*, vol. 2, no. 2, pp. 1-43, 1998.
- [55] S. Jain, "Communication of signals and responses leading to cell survival / cell death using Engineered Regulatory Networks", *PhD Thesis, Jaypee University of Information Technology*, Solan, Himachal Pradesh, India, 2012.
- [56] S. Jain and P. K. Naik, "System Modeling of cell survival and cell death: A deterministic model using Fuzzy System", *International Journal of Pharma and Bio Sciences (IJPBS)*, vol.3, no. 4, pp. 358-373, 2012.
- [57] S. Jain, and D. S. Chauhan, "Linear and Non Linear Modeling of Protein Kinase B/ AkT", *International Conference on Information and Communication Technology for Sustainable Development (ICT4SD - 2015)*, Ahmedabad, India.
- [58] S. Jain, and D. S. Chauhan, "Mathematical Analysis of Receptors For Survival Proteins", *International Journal of Pharma and Bio Sciences (IJPBS)*, vol.6, no. 3, pp. 164-176, 2015.
- [59] C. J. C. Burges, "A tutorial on support vector machines and probabilistic neural network for pattern recognition", *Data Min Knowl Disc*, vol. 2, no. 2, pp. 1-43, 1998.
- [60] S. Jain, "Mathematical Analysis and Probability Density Function of FKHR pathway for Cell Survival /Death", *Control System and Power Electronics – CSPE 2015*, Bangalore, Aug 1-2, 2015.
- [61] S. Jain, P. K. Naik, and S. V. Bhooshan, "Nonlinear Modeling of cell survival/ death using artificial neural network", *International Conference on Computational Intelligence and Communication Networks (CICN2011)*, Gwalior, India, Oct 07-09, 2011, pp. 565-568.

- [62] J. Virmani, V. Kumar, N. Kalra, and N. Khandelwal, “SVM-based characterization of liver cirrhosis by singular value decomposition of GLCM matrix”, *International Journal of Artificial Intelligence and Soft Computing*, vol. 3, no. 3, pp. 276-296, 2013.
- [63] A. E. Hassanien, N. E. Bendary, M. Kudelka, and V. Snasel, “Breast cancer detection and classification using support vector machines and pulse coupled neural network”, *In Proceedings of 3rd International Conference on Intelligent Human Computer Interaction IHCI 2011*, Prague, Czech Republic, 2011, pp. 269-279.
- [64] A. T. Azar and S. A. El-Said, “Performance analysis of support vector machine classifiers in breast cancer mammography recognition”, *Neural Computing and Applications*, vol. 24, pp. 1163-1177, 2014.
- [65] S. Rana, S. Jain, and J. Virmani, “Classification of Kidney Lesions using Gabor Wavelet Texture Features”, *In Proceedings of the 10th INDIACom 3rd 2016 International Conference on Computing for Sustainable Global Development*, New Delhi, 16th –18th March, 2016, pp. 2528-2532.
- [66] Kriti, J. Virmani, N. Dey, and V.Kumar, “PCA-PNN and PCA-SVM based CAD systems for breast density classification”, *In Applications of Intelligent Optimization in Biology and Medicine: Current Trends and Open Problems*, 2015, vol. 96, pp. 159-180.
- [67] S. Jain, “Regression analysis on different mitogenic pathways”, *Network Biology*, June vol. 6, no. 2, pp. 40-46, 2016.
- [68] S. Jain, “Mathematical Analysis using Frequency and Cumulative Distribution functions for Mitogenic Pathway”, *Research Journal of Pharmaceutical, Biological and Chemical Sciences*, May- June 2016, vol.7, no. 3, 2016.
- [69] S. Bhusri, S. Jain, and J. Virmani, “Classification of Breast Lesions based on Laws’Feature Extraction Techniques”, *In Proceedings of the 10th INDIACom 3rd 2016 International Conference on Computing for Sustainable Global Development*, New Delhi, 16th–18th March, 2016, pp. 2528-2532.
- [70] S. Bhusri, S. Jain, and J. Virmani, “Breast Lesions Classification using the Amalgamation of morphological and texture features”, *International Journal of Pharma and Bio Sciences*, Apr-Jun, vol. 7, no. 2, pp. 617-624, 2016.

[71] S. Rana, S. Jain, and J. Virmani, "SVM-Based Characterization of Focal Kidney Lesions from B-Mode Ultrasound Images", *Research Journal of Pharmaceutical, Biological and Chemical Services*, vol. 7, no. 4, 2016.

[72] I. Kumar, H. S. Bhadauriab, and J. Virmani, "Wavelet Packet Texture Descriptors based four-class BIRADS Breast Tissue Density Classification", *4th International Conference on Eco-friendly Computing and Communication Systems, Procedia Computer Science 70*, 2015, pp. 76 – 84.

Appendix-A

Texture Features Used in the Present Work

A.1 Statistical Texture Features

A.1.1 First Order Statistics (FOS)

For the individual pixel values x_i , the computed features are given as:

$$\text{Mean} = \frac{1}{N} \sum_i x_i$$

$$\text{Standard Deviation} = \frac{(\sum_i (x_i - \bar{x})^2)}{\sqrt{N - 1}}$$

$$\text{Third Moment} = \frac{\sum_i (x_i - \bar{x})^3}{N\sigma^3}$$

$$\text{Uniformity} = \sum_i p(i)^2$$

$$\text{Entropy} = - \sum_i p(x_i) \log p(x_i)$$

$$\text{Smoothness} = 1 - \frac{1}{1 + \sigma^2}$$

A.1.2 Second Order Statistics (GLCM Features)

$$\text{Angular Moment} = \sum_{i,j} P_{i,j}^2$$

$$\text{Contrast} = \sum_{i,j} P_{i,j} (i - j)^2$$

$$\text{Correlation} = \sum_{i,j} P_{i,j} \left[\frac{(i - \mu_i)(j - \mu_j)}{\sigma_i \sigma_j} \right]$$

$$\text{Variance} = \sum_{i,j} P_{i,j} (i - \mu_i)^2$$

$$\text{Inverse Difference Moment} = \sum_{i,j} \frac{P_{i,j}}{1 + (i - j)^2}$$

$$\text{Sum Average} = f_{12} = \sum_{i=2}^{2Ng} i p_{x+y}(i)$$

$$\text{Sum Entropy} = f_{14} = - \sum_{i=2}^{2Ng} p_{x+y}(i) \log(p_{x+y}(i))$$

$$\text{Sum Variance} = f_{13} = \sum_{i=2}^{2Ng} (i - f_{14})^2 p_{x+y}(i)$$

$$\text{Entropy} = - \sum_{i,j} p_{i,j} \log(p_{i,j})$$

$$\text{Difference Entropy} = f_{16} = - \sum_{i=0}^{Ng-1} p_{x-y}(i) \log(p_{x-y}(i))$$

$$\text{Difference Variance} = - \sum_{i=0}^{Ng-1} (i - f_6)^2 p_{x-y}(i)$$

Where $f_6 = \sum_{i,j} |i - j| p_{i,j}$

A.1.3 Higher Order Statistics (GLRLM Features)

$$\text{Short Run Emphasis} = \frac{\sum_{i=1}^G \sum_{j=1}^R \frac{p(i,j|\theta)}{j^2}}{\sum_{i=1}^G \sum_{j=1}^R p(i,j|\theta)}$$

$$\text{Long Run Emphasis} = \frac{\sum_{i=1}^G \sum_{j=1}^R p(i,j|\theta) * j^2}{\sum_{i=1}^G \sum_{j=1}^R p(i,j|\theta)}$$

$$\text{Low Gray Level Run Emp} = \frac{\sum_{i=1}^G \sum_{j=1}^R \frac{p(i,j|\theta)}{i^2}}{\sum_{i=1}^G \sum_{j=1}^R p(i,j|\theta)}$$

$$\text{High Gray level Run Emp.} = \frac{\sum_{i=1}^G \sum_{j=1}^R p(i,j|\theta) * i^2}{\sum_{i=1}^G \sum_{j=1}^R p(i,j|\theta)}$$

$$\text{Short Run High Gray Emp} = \frac{\sum_{i=1}^G \sum_{j=1}^R \frac{p(i,j|\theta) \times i^2}{j^2}}{\sum_{i=1}^G \sum_{j=1}^R p(i,j|\theta)}$$

$$\text{Short Run Low Gray Emp} = \frac{\sum_{i=1}^G \sum_{j=1}^R \frac{p(i,j|\theta)}{i^2 \times j^2}}{\sum_{i=1}^G \sum_{j=1}^R p(i,j|\theta)}$$

$$\text{Long Run High Gray Emp} = \frac{\sum_{i=1}^G \sum_{j=1}^R \frac{p(i,j|\theta) \times j^2}{i^2}}{\sum_{i=1}^G \sum_{j=1}^R p(i,j|\theta)}$$

$$\text{Gray level non Uniformity} = \frac{\sum_{i=1}^G \left(\sum_{j=1}^R p(i,j|\theta) \right)^2}{\sum_{i=1}^G \sum_{j=1}^R p(i,j|\theta)}$$

$$\text{Run Leng non Uniformity} = \sum_{j=1}^R \left(\sum_{i=1}^G p(i,j|\theta) \right)^2 / \sum_{i=1}^G \sum_{j=1}^R p(i,j|\theta)$$

$$\text{Run Percentage} = \sum_{i=1}^G \sum_{j=1}^R p(i,j|\theta) / n$$

A.1.4 Other Statistics Features (GLDS Features)

$$\text{Homogeneity} = \sum_{i,j} \frac{P_{i,j}}{1 + (i - j)^2}$$

$$\text{Contrast} = \sum_{i,j} P_{i,j} (i - j)^2$$

$$\text{Energy} = \sqrt{\sum_{i,j} P_{i,j}^2}$$

$$\text{Entropy} = - \sum_{i,j} P_{i,j} \log (P_{i,j})$$

$$\text{Mean} = \frac{1}{m} \sum_{i,j} i P_{i,j}$$

A.2. Spatial Filtering Based Texture Features

A.2.1 Laws' Texture Features

Laws' masks of lengths 3, 5, 7 and 9 are used to calculate different features. A description of these masks is given below.

Table 1: Description of Laws' masks of different lengths

Length of 1-D filter	1-D filter coefficients	No. of 2D Laws' masks	No. of TR images
3	L3=[1, 2, 1] E3=[-1, 0, 1] S3=[-1, 2, -1]	9	6
5	L5= [1, 4, 6, 4, 1] E5= [-1, -2, 0, 2, 1] S5= [-1, 0, 2, 0, -1] W5= [-1, 2, 0, -2, 1] R5= [1, -4, 6, -4, 1]	25	15
7	L7= [1, 6, 15, 20, 15, 6, 1] E7= [-1 -4, -5, 0, 5, 4, 1] S7= [-1, -2, 1, 4, 1, -2, -1]	9	6
9	L9= [1, 8, 28, 56, 70, 56, 28, 8, 1] E9= [1, 4, 4, -4, -10, -4, 4, 4, 1] S9= [1, 0, -4, 0, 6, 0, -4, 0, 1] W9= [1, -4, 4, -4, -10, 4, 4, -4, 1] R9= [1, -8, 28, -56, 70, -56, 28, -8, 1]	25	15

Note: TR: rotation invariant texture images.

As an example Laws' mask of length 5 is used for explanation purposes. The AOIs are convolved with each of the above twenty five 2D Laws' masks.

a) The Texture Image (TI) is obtained by convolving the input image $I(i, j)$ with the 2-D mask

$$TI_{E5E5} = I_{i,j} \otimes E5E5$$

b) The contrast of the texture image obtained from above equation is normalized

$$Normalize(TI_{mask}) = \frac{TI_{mask}}{TI_{L5L5}}$$

c) The Texture Energy Measurement (TEM) filters are used to pass the Texture image

$$TEM_{i,j} = \sum_{u=-5}^5 \sum_{v=-5}^5 Normalize(TI_{i+u,j+v})$$

d) To obtain 15 rotationally invariant TEM's that are denoted as TR are obtained by collaborating the 25 TEM descriptors

$$TR_{E5L5} = \frac{TEM_{E5L5} + TEM_{L5E5}}{2}$$

e) Five statistical parameters are determined, that are the Mean, Standard Deviation, Skewness, Kurtosis, Entropy. Here $M \times N$ is the dimension of the image

1) *Mean (m)*: It describes the mean intensity value with in texture image.

$$Mean = \frac{\sum_{i=0}^M \sum_{j=0}^N (TR_{i,j})}{M \times N}$$

2) *Standard Deviation (SD)*: It is used to measure the variability.

$$SD = \sqrt{\frac{\sum_{i=0}^M \sum_{j=0}^N (TR_{i,j} - Mean)^2}{M \times N}}$$

3) *Skewness*: It measures of the asymmetry of the probability distribution of a random variable that is real valued.

$$Skewness = \frac{\sum_{i=0}^M \sum_{j=0}^N (TR_{i,j} - Mean)^3}{M \times N \times SD}$$

4) *Kurtosis*: It measures of the probability distribution shape of a random variable that is real valued.

$$Kurtosis = \frac{\sum_{i=0}^M \sum_{j=0}^N (TR_{i,j} - Mean)^4}{M \times N \times SD^4} - 3$$

5) *Entropy*: It measures the randomness of the elements of the image.

$$Entropy = \frac{\sum_{i=0}^M \sum_{j=0}^N (TR_{i,j})^2}{M \times N}$$

A.3. Spectral Based Texture Features

A.3.1 Gabor Filter Based Methods

$$Mean = \frac{1}{m} \sum_{i,j} i P_{i,j}$$

$$Variance = \sum_{i,j} P_{i,j} (i - \mu_i)^2$$

A.3.2 FPS Feature

$$\textit{Radial Sum} = \sum_{r_1^2 < u^2 + v^2 < r_2^2} |F(u, v)|^2$$

$$\textit{Angular Sum} = \sum_{\theta_1 \leq \tan^{-1} \frac{v}{u} \leq \theta_2} |F(u, v)|^2$$

